AD NUMBER

AD484494

LIMITATION CHANGES

TO:

Approved for public release; distribution is unlimited.

FROM:

Distribution authorized to U.S. Gov't. agencies and their contractors; Critical Technology; JUN 1966. Other requests shall be referred to Air Force Aero Propulsion Laboratory, Research and Technology Division, Wright-Patterson AFB, OH 45433. This document contains export-controlled technical data.

AUTHORITY

afapl ltr, 12 apr 1972

Seventh Quarterly Technical Progress Report On Investigation of Hermetically Sealed Maintenance-Free, High Rate, Nickel-Cadmium Batteries for Aircraft Applications

June, 1966

Air Force Aero Propulsion Laboratory
Research and Technology Division
Air Force Systems Command, USAF
Wright-Patterson Air Force Base, Ohio 45433

Project No. 8173
Task No. 817304

Prepared Under Contract No. AF33(615)-2087
by
Gulton Industries, Inc.
Alkaline Battery Division
Metuchen, New Jersey

Authors: E. Kantner, P. Ritterman, R.V. Tarantino and R. C. Shair

NOTICES

Foreign announcement and distribution of this report is not authorized.

The distribution of this report is limited because it contains technology identifiable with items on the strategic embargo list excluded from export or re-export under U. S. Export Control Act of 1949 (63 STAT. 7), as amended (50 USC App. 2020, 2031), as implemented by AFR 400-10.

The work covered by this report was accomplished under Air Force Contract AF33(615)-2087, but this report is being published and distributed prior to Air Force review. The publication of this report, therefore, does not constitute approval by the Air Force of the findings or conclusions contained herein. It is published for the exchange and stimulation of ideas.

TABLE OF CONTENTS

TABLES

LIST OF FIGURES

LIST OF FIGURES continued

I. ABSTRACT

High rate discharges were carried out at -30°F, -20°F, -10°F and 0°F using the 35 AH laboratory prototype cell. Cell voltages at the end of one minute of discharge were 0.45 V, 0.55 V, 0.68 V and 0.79 V respectively.

Cell behavior during high rates of charging was also investigated at -30°F, -20°F, -10°F, 0°F, +10°F, +20°F, 32°F, 77°F and 140°F. At temperatures below +20°F, the cell evolved hydrogen when charged at 350 amperes for five minutes. This hydrogen evolution occurred only during the initial portion of charging. Oxygen evolution occurred in the latter part of charging at all temperatures based on these gassing phenomena.

The parasitic currents (i.e. the portions of charge current which do not contribute to the stored chemical energy of the cell) were calculated at temperatures of -30°F to 140°F. The actual ampere-hour inputs at these temperatures were then determined as a function of time.

The Adhydrode®, as a charge control device, was studied during high rates of charging at all temperatures. However, on a 600 ampere discharge, the Adhydrode voltage increased due to the heat generated during the discharge.

A series of constant potential charges were carried out at -30°F

using charging voltages of 1.65 V, 1.8 V, 1.9 V and 1.95 V. The currents produced at these voltages were insufficient to charge the cell in five minutes. Also, hydrogen evolution occurred at charging voltages of 1.9 V or greater.

A Cd-Cd $(OH)_2$ coulometer was tested at high currents and temperatures of 20°F and 140°F. The coulometer was found to yield a premature signal at 20°F.

Assembly of cells for the 22 AH battery is in progress. Electrical formation of the battery plates has been completed. Samples of cell hardware have been received and approved. The first laboratory prototype of the 22 AH cells has been assembled and is being tested. The cell was subjected to the charge-discharge duty cycle at room temperature. Testing at high and low temperatures is in progress.

The design of the parallel chopper charge control-charge conditioning system was completed and selected as the most promising for aircraft applications where a "boost-only" system is required.

II. INTRODUCTION

The objectives of this research and development program are to design, develop and fabricate hermetically sealed, maintenance-free, high rate, nickel-cadmium batteries for aircraft applications. That is, the battery must be capable of delivering the necessary power for engine starting, it must be capable of withstanding the varied enviromental conditions that may prevail in an aircraft, and it must be compatible with the constant potential charging system of the aircraft. To achieve these objectives, two broad areas are being investigated.

Firstly, a basic research program has been undertaken with the ultimate goal of improving the electrochemical operation of sealed nickel-cadmium cells. The areas where improvements are sought include longer shelf life, better electrical performance at high rates of charge and discharge, and better electrical performance at high and low temperature extremes.

Secondly, to make the battery compatible with the constant potential charging system of the aircraft, a charge control-charge conditioning system is being studied to allow rapid charging of the battery when it needs to be recharged. When the battery becomes fully charged, the charge control-charge conditioning system must also be capable of terminating the charging current on signal from an end-of-charge signal generating device, such as a coulometer, Adhydrode or

pressure switch.

The report describes the work performed during the Seventh Quarter of this program. Details of this work are presented in the following Sections.

III. BATTERY RESEARCH AND DEVELOPMENT

A. THEORY OF ELECTROCHEMICAL PROCESSES OCCURRING DURING HIGH RATE CHARGING

The reactions occurring in a nickel-cadmium cell during charge can be represented by the following equation:

(1) $2\,Ni(OH)_2 + Cd(OH)_2 \longrightarrow 2\,Ni\,OOH + Cd + 2\,H_2O$

At the individual electrodes the reactions are

(2) $Cd(OH)_2 + 2e^- \longrightarrow Cd + 2\,OH^-$ (-0.809 V)

at the negative, and

(3) $2\,Ni(OH)_2 + 2\,OH^- \longrightarrow 2\,Ni\,OOH + 2H_2O + 2\,e^-$ (0.49 V)

at the positive.

A competing reaction at the negative electrode causes the evolution of hydrogen

(4) $2\,H_2O + 2\,e^- \longrightarrow H_2 + 2\,OH^-$ (-0.828 V)

Similarly, at the positive electrode oxygen is evolved

(5) $4\,OH^- \longrightarrow O_2 + 2\,H_2O + 4\,e^-$ (0.401 V)

Reactions (2) and (3) are considered "useful" because they produce stored energy which is readily useable. By the same definition reactions (4) and (5) are considered parasitic. The values in the parantheses are the E°, the standard half-cell potentials, for the particular reaction as given in W. D. Latimer's "Oxidation Potentials".

According to the E° values, reaction (5) is favored over (3)

when charging a nickel-cadmium cell. The oxygen overvoltage is of such magnitude that this trend is reversed. However, overvoltage is current and temperature dependent. It increases with increasing current density and decreasing temperature. Thus, under certain conditions, such as low charging rates and/or elevated temperatures, the potential at the positive electrode may be such that there can be two competing reactions. This helps to explain why oxygen evolution is observed at the positive electrode at very low charging rates and/or at elevated temperatures. There is still another condition where oxygen evolution is favored and that is due to polarization which is discussed below.

From the E° values, reaction (2) is favored over (4) during charge. Considering hydrogen over voltage, this situation becomes even more favorable. However, polarization increases with increasing current density and decreasing temperature. Thus, here too, there may exist a condition where, due to polarization, the potential at the negative is such that there can be two competing reactions. Consequently, at low temperatures and high rates of charge, hydrogen evolution is increasingly favored.

B. EXPERIMENTAL PROCEDURES AND RESULTS

1. High Rate Discharge Characteristics

600 ampere discharges were carried out at -30°F, -20°F,

-10°F and 0°F using the 35 AH laboratory prototype cell. These experiments were carried out to determine the lowest temperature at which the cell voltage was above 0.74 V after one minute of discharge.

Prior to each discharge, the cell was charged at 35 amperes until a rapid rise in cell pressure was noted (72-74 minutes). Following this room temperature charge, the cell was soaked at the test temperature for five hours and then discharged at 600 amperes. The cell was then shorted overnight with a 0.5 ohm resistor before the next 35 ampere charge.

The results of these experiments are shown in Figure 1. As may be seen, the cell met the requirements at 0°F under these test conditions. Cell voltages at the end of one minute were 0.45 V, 0.55 V, 0.7 V and 0.78 V at -30°F, -20°F, -10°F and 0°F respectively.

High rate discharges were also carried out at low temperatures following a 350 ampere charge for five minutes. Here the cell was soaked in the fully discharged condition, at the test temperature, overnight, before being charged at 350 amperes. Following the charging, the cell was immediately discharged at 600 amperes. While charging and discharging, the cell was maintained in a constant temperature environment. Figure 2 shows the results of these experiments at -30°F and +10°F. As may be seen, the two discharge curves are quite

similar even though the temperatures differed. This was probably due to the cell temperature being higher than that of its environment as a result of the high rate charging. These data also indicate that under these test conditions the discharge requirements were met even at -30°F.

2. High Rate Charge Characteristics

Data was obtained on the high rate charge characteristics of the 35 AH prototype cell at temperatures from -30°F to 72°F. Before charging, the cell was soaked in a constant temperature chamber overnight, in the fully discharged condition. Charging was done at a constant current of 350 amperes for five minutes with cell voltage and pressure being monitored. These data are shown in Figures 3 and 4. Figure 3 shows that during the initial portion of charge, cell voltage is high at the low temperatures. It is while the voltage is high that a rapid rise in cell pressure occurs, as shown in Figure 4. The fact that the Adhydrode was insensitive to this rapid rise in pressure suggests that the gas was hydrogen. This was substantiated by analyzing the gas in the cell with a Burrel Gas Analyzer. This means that, when charging at low temperature, polarization takes place initially at the negative electrode. As charging proceeds, the gassing stops until the end of charge is approached. Then oxygen is evolved at the positive electrode. This interpretation is in agreement with the observed data shown in

Figures 4 and 5. The data in Figure 5 were obtained using a 0.5 ohm resistor between the Adhydrode and negative plates. Before charging, the Adhydrode signal was zero. When the charging current was turned on, the Adhydrode signal rose sharply to 2-3 mv and was stable at that value until the cell approached end of charge. Then the signal increased linearly with time, and as may also be seen from Figure 4, linearly with pressure.

When charging the cell at -30°F at 350 amperes, initial cell voltage was high (above 2 V) and cell pressure rose rapidly. (Cell pressure was about 75 psi within two minutes and, consequently, charging was terminated.) In an attempt to reduce this rapid rise in pressure, the cell was charged at -30°F using a constant potential charging mode. Figure 6 shows a plot of charging current at several voltages when the cell was charged in a constant potential mode at -30°F. These data indicate that, at this low temperature, the current was insufficient to charge the cell in five minutes. Also, at charging voltages of 1.90 V or higher, hydrogen was evolved.

3. Parasitic Current and Charge Efficiency

The high, initial pressure rise encountered when the cell was charged rapidly at low temperatures promoted an investigation of charge efficiency at the high charging rate. Consequently, the parasitic current of the 35 AH cell was determined during various stages of its charge

at 350 amperes, at various temperatures from -30°F to 140°F. The void volume of the cell had been previously determined as 133 cc. This information, along with the gassing rate and a knowledge of the species of the gas evolved, enabled calculating the parasitic current.

The number of moles of gas present at a particular temperature is given by $\eta = \frac{PV}{RT}$ where

P = Pressure in atmosphere

V = Volume in liters

T = Absolute temperature

R = .082 liter-atm/degree K

The two reactions which produce gas within the cell are:

(4) $2H_2O + 2e^- \longrightarrow H_2 + 2\,OH^-$, and

(5) $4\,OH^- \longrightarrow O_2 + 2H_2O + 4e^-$

For each mole of hydrogen produced, 2 x 96500 coulombs are required, while for oxygen, 4 x 96500 coulombs are necessary. Expressed in ampere-hours, these correspond to 53.6 and 107.2 respectively.

A relationship between current and rate of pressure increase was derived from the equations above. These are

$$I_{H_2} = \frac{\eta 53.6}{\text{time in hours}} \quad \text{and}$$

$$I_{O_2} = \frac{\eta 107.2}{\text{time in hours}}$$

Since η can be expressed as

$$\eta = \frac{\frac{P\text{lbs}}{15}}{(.082)(T)} V$$

$$(6)\quad I_{H_2} = \frac{\frac{P}{15}\ 0.133}{(0.082)(T)t}\ 53.6 = \frac{P}{Tt}\ (5.8)$$

$$(7)\quad I_{O_2} = \frac{\frac{P}{15}\ 0.133}{(.082)(T)t}\ 107.2 = \frac{P}{Tt}\ (11.6)$$

During the initial part of charge, equation (6) was applied and at the end of charge, equation (7) was applied. The calculations were based on the assumption that only hydrogen was produced at the beginning of charge and only oxygen at the end.

The parasitic currents obtained during charge, at various temperatures, at 350 amperes, are given in Table I. Large parasitic currents are shown early in the charge for low temperatures. At 20°F and above the initial parasitic current is practically zero. 100% efficiency would correspond to an input of 29.17 AH in 5 minutes of charge. Actual inputs ranged from 29.01 AH to 26.67 AH.

4. Cd/Cd(OH)$_2$ Coulometer Studies

The behavior of the Cd/Cd(OH)$_2$ coulometer was evaluated at 20°F and 140°F, the temperature range in which the 35 AH cell was found capable of being charged at 350 amperes without evolving hydrogen. As is shown in Figure 7, the coulometer gave a premature signal at 20°F. The signal (1.0V) was reached after a 15 AH input at 20°F and 27.4 AH at 140°F. On "discharge" (at 600 amperes), the signal was obtained at 22.7 AH. This is shown in Figure 8. The difference between the input and output signal was 4.7 AH. This difference of 4.7 AH was

TABLE I

PARASITIC CURRENT VS. CHARGE TIME ON 350 AMPERE CHARGE AT VARIOUS TEMPERATURES

TEMPERATURE: -30°F

0	to	0.5 min.	210 amperes	
0.5	to	1 "	190 "	
1	to	1.25 "	81.5 "	
1.25	to	2.75 "	12.7 "	

TEMPERATURE: -20°F

0	to	0.25 min.	170 amperes	42.5 amp-min.
0.25	to	0.5 "	85 "	21.25 "
0.5	to	0.75 "	40 "	10 "
0.75	to	1.75 "	2.84 "	2.84 "
1.75	to	2 "	5.68 "	1.42 "
2	to	5 "	16.1 "	48.3 "
				126.31 "

TEMPERATURE: -10°F

0	to	0.1 min.	174 amperes	17.4 amp-min.
0.1	to	0.25 "	165 "	24.8 "
0.25	to	0.5 "	55.6 "	13.9 "
0.5	to	0.75 "	27.8 "	6.95 "
0.75	to	1.25 "	0 "	0 "
1.25	to	2 "	7.4 "	5.55 "
2	to	5 "	29	87 "
				155.60 "

TABLE I - continued

TEMPERATURE: 0°F

0	to 0.1 min.	78 amperes	7.8 amp-min.	
0.1	to 0.25 "	137 "	20.6 "	
0.25	to 0.5 "	26.5 "	6.6 "	
0.5	to 2.5 "	0 "	0 "	
2.5	to 3.5 "	16 "	16 "	
3.5	to 5 "	24 "	36 "	
			87.0 "	

TEMPERATURE: +10°F

0	to 0.1 min.	60 amperes	6 amp-min.	
0.1	to 0.4 "	26.6 "	8 "	
0.4	to 0.6 "	8 "	1.6 "	
0.6	to 2.75 "	0 "	0 "	
2.75	to 3.50 "	7 "	5.25 "	
3.5	to 5 "	10 "	15 "	
			35.85 "	

TEMPERATURE: +20°F

0	to 0.1 min.	0 amperes	0 amp-min.	
0.1	to 0.25 "	13 "	1.95 "	
0.25	to 0.5 "	15.2 "	3.8 "	
0.5	to 2 "	0.9 "	1.35 "	
2	to 2.5 "	0 "	0 "	
2.5	to 3.5 "	2.6 "	2.6 "	
3.5	to 4.5 "	8 "	8 "	
4.5	to 5 "	16 "	8 "	
			25.70 "	

TABLE I - continued

TEMPERATURE: 32°F

0	to	3.25 min.	0 amperes	0	amp-min.
3.25	to	4.25 "	7 "	7	"
4.25	to	5 "	17 "	12.75	"
				19.75	"

TEMPERATURE: +72°F

0	to	3.25 min.	0 amperes	0	amp-min.
3.25	to	4.25 "	5 "	5	"
4.25	to	5 "	9.3 "	7	"
				12	"

TEMPERATURE: +140°F

0	to	1.25 min.	0 amperes	0	amp-min.
1.25	to	2 "	4.32 "	3.23	"
2	to	3 "	7.54 "	7.54	"
3	to	4 "	37 "	37	"
4	to	5 "	52.1 "	52.1	"
				99.87	"

due to the difference in charging and discharging rates. The input was at 350 amperes whereas the output was measured at 600 amperes. The rate dependence of the timing of the signal coupled with the observation that the coulometer gave a premature signal at low temperature, could cause an imbalance between it and the battery. This imbalance could either prevent the battery from fully charging by giving a premature signal, or cause the battery to overcharge at a high rate by giving a delayed signal.

C. BATTERY DESIGN AND FABRICATION - 22 AH BATTERY

1. Assembly

Electrical formation of approximately 6000 plates for a 22 AH battery was completed. The formation procedure consisted of three charge-discharge cycles with the cells being flooded and vented. Both positive and negative plate capacities were checked during the discharge portion of the formation procedure. After the third discharge, the plates were washed, dried and inspected.

Auxiliary tabs, 0.015" nickel, were welded to the plate tabs and trimmed to size. This operation was completed on all the battery plates.

Samples of all cell hardware have been received for inspection and approval. These were cell cases, top and bottom covers, terminals, combs, and plate supports. All samples have been approved and all

hardware has been received.

2. Testing of 22 AH Cells

Assembly of 22 AH cells for battery fabrication is in progress. The first laboratory prototype cell (LP-1) was subjected to the duty cycle at room temperature. This cycle consisted of the following:

1. 600 ampere discharge for one minute.
2. 220 ampere charge.
3. 600 ampere discharge for one minute.
4. 220 ampere charge.
5. 22 ampere discharge to 1.0 volts.

The results of these tests are shown in Figures 9 to 13.

After adding 90 cc of 34% KOH, the cell was sealed without evacuating. It was charged at C/10 for 24 hours and discharged at 22 amperes to 1.0 V. The steady-state overcharge pressure was 12 psi and capacity about 25 AH. The cell was then charged at the one-hour rate (22 amps) until the voltage and pressure started to rise (this occurred at 66 min.). The cell was then discharged at 600 amperes for one minute. The current density during discharge was 1.42 amp/sq. inch. These results are shown in Figure 9. Cell voltage at one minute was 0.89 V. The cell was then charged, with no rest time, at 220 amperes just long enough to return 10 AH. In 2.6 minutes, cell voltage rose to 1.59 V and pressure rose from 5.5 psi to 9.5 psi, as shown

in Figure 10. The cell was again discharged at 600 amperes for one minute with no rest time. Voltage at one minute was again 0.89 V, as shown in Figure 11. The cell was again charged at 220 amperes, this time until voltage and pressure started rising, as shown in Figure 12. This required about a 115% input based on the capacity removed on the previous discharge. The following discharge, at 22 amperes, yielded 23.8 AH to 1.0 V, as shown in Figure 13. The pressure rise during these tests was due to oxygen, as evidenced by the fact that, after an overnight stand, the pressure gauge indicated about a five inch vacuum. These data indicate that the cell has the required high rate capability. During these high rate tests no part of the cell reached a temperature where it was uncomfortable to the touch, indicating that the present cell design is sound.

D. THERMAL ANALYSES OF THE 22 AH AND 35 AH BATTERIES

Because of the high rate charge and discharge requirements, analyses were made of the temperature rise that might be expected in the battery during high rate cycling. These analyses were made both for the 22 AH and 35 AH battery. Because of the complexity of the problem, computations were made assuming that the heat generated is due solely to I^2R heating, and that no heat is lost to the environment during the cycle. The last assumption represents the worst condition.

1. Analyses of Temperature Rise During Cycles

Table II below summarizes the cycle that the battery will encounter.

TABLE II

CHARGE-DISCHARGE DUTY CYCLE

Step No.	Description	Rate (Amps)	Time (Min.)
1	Discharge	600	1
2	Charge *	220	3
	Rest	---	2
3	Discharge	600	1
4	Charge	220	3
	Rest	---	2
5	Rest	---	60
6	Discharge	11	130
7	Charge	220	5
8	Rest	---	240
		TOTAL TIME	447 MIN.

* A 220 amp., 3 minute charge represents the worst case thermally, since we are assuming that the heat generated is a function of I^2.

A thermal analysis has been made solely on the basis of power dissipated as a result of I^2R, where I is the current flowing through the cell and R is its internal resistance.

In normal (low rate) routines, the analysis of heat is made through an application of the first law of thermodynamics, and I^2R losses are negligible. At high rates, however, I^2R losses are predominent and the power dissipated through Δ work is negligible by comparison.

Table II may be extended to show the power dissipated during each step. Using $R_{cell} = 5 \times 10^{-4}$ ohms, the following values for I^2R are obtained.

TABLE III

ENERGY LOSSES DURING CYCLE

Step No.	I	I^2R	Time (Hrs.)	Watt Hours
1	600	180	1/60	3.0
2	220	24	3/60	1.2
3	600	180	1/60	3.0
4	220	24	3/60	1.2
5	0	---	---	0
6	11	.0605	130/60	.131
7	220	24	5/60	2.0
			TOTAL	10.53

Considering the cycle in sections, Steps 1-4 represent section I; steps 6-7, section 2.

Utilizing $q = mC_p\Delta T$ and the power dissipated as shown in

Table III, we are able to determine the Δ T due to the heat generated.

$q_{section\ 1} = 8.4$ watthours x 3.41 $\frac{BTU/Hr}{watt}$ = 28.8 BTU

$q_{section\ 2} = 2.13$ watthours x 3.41 $\frac{BTU/Hr}{watt}$ = 7.25 BTU

$m = 2.5$ lbs.

$C_p = .252 \frac{BTU}{\#\,°F}$

$\Delta T_{sect.\ 1} = \frac{q1}{mC_p} = \frac{28.8}{2.5(.252)} = 46°F$

$\Delta T_{sect.\ 2} = \frac{q2}{mC_p} = \frac{7.25}{2.5(.252)} = 11.5°F$

Hence, total temperature rise during one complete cycle should be 57.5°F if no heat losses occur.

2. Analyses of Temperature Gradients

Figure 14 shows a heat sink fin from the center of the battery stack. Using a network nodal analysis for the nine points on the fin, utilizing the fact that the summation of heat flow to any node equals zero and that

$T_1 = T_7$, $T_2 = T_8$, $T_3 = T_6 = T_9 = 0$,

we get the following equations which enable one to establish the thermal gradients:

Nodal Point	Equation
1	$q_{cell} + q_{2-1} + q_{4-1} = 0$
2	$q_{cell} + q_{1-2} + q_{3-2} + q_{5-2} = 0$
3	$q_{cell} + q_{2-3} + q_{6-3} + q_{CB\,(conducted\ from\ batt.)} = 0$
4	$q_{cell} + q_{1-4} + q_{5-4} + q_{7-4} = 0$

$$5 \qquad q_{cell} + q_{4-5} + q_{2-5} + q_{6-5} + q_{8-5} = 0$$

$$6 \qquad q_{cell} + q_{5-6} + q_{3-6} + q_{9-6} + q_{CB} = 0$$

$$q = KA \frac{dT}{dX} = KA \frac{\Delta T}{\Delta X}$$

$$K = 120 \frac{BTU}{Hr\ Ft}$$

$$\frac{A}{\Delta X} = \frac{Lb}{2W} \text{ in X direction and } \frac{Wb}{2L} \text{ in Y direction}$$

and $W = 3.12$ in. $= .26$ ft.

$b = .062$ in. $= .005$ ft.

$L = 7.12$ in. $= .59$ ft.

$$\frac{KLb}{2W} = .675$$

$$\frac{KWb}{2L} = .135$$

Rewriting equations 1 to 6:

A. $q_{cell} + .135(T_2 - T_1) + .675(T_4 - T_1) = 0$

$q_{cell} - .135T_1 - .675T_1 + .35T_2 + .675T_4 = 0$

$q_{cell} - .810T_1 + .135T_2 + .675T_4 = 0$

B. $q_{cell} + .135(T_1 - T_2) + .135(T_3 - T_2) + .675(T_5 - T_2) = 0$

$q_{cell} + .135T_1 - .135T_2 - .135T_2 - .675T_2 + .135T_3 + .675T_5 = 0$

$q\ cell + .135T_1 - .945T_2 + .135T_3 + .675T_5 = 0$

$q\ cell + .135T_1 - .945T_2 + .675T_5 = 0$

C. $q_{cell} + .135(T_2 - T_3) + .675(T_6 - T_3) + q_{CB} = 0$

$q_{cell} + .135T_2 + q_{CB} = 0$

D. $q_{cell} + .135(T_5 - T_4) + .675(T_1 - T_4) + .675(T_7 - T_4) = 0$

$q_{cell} + 1.35T_1 - .135T_4 - .675T_4 - .675T_4 + .135T_5 = 0$

$q_{cell} + 1.35T_1 - 1.485T_4 + .135T_5 = 0$

E. $q_{cell} + .135(T_4 - T_5) + .135(T_6 - T_5) + .675(T_2 - T_5) + .675(T_8 - T_5) = 0$

$q_{cell} + .675T_2 + .135T_4 - .135T_5 - .135T_5 - .675T_5 - .675T_5 + .135T_6 + .675T_8 = 0$

$q_{cell} + 1.35T_2 + .135T_4 - 1.62T_5 = 0$

F. $q_{cell} + .135T_5 - .135T_6 + .675T_3 - .675T_6 + .675T_9 - .675T_6 + q_{CB} = 0$

$q_{cell} + .135T_5 + q_{CB} = 0$

Equation C may be rewritten as

$$T_2 = -7.5 \left[q_{cell} + q_{CB}\right] \qquad \text{I.}$$

and since equation F may be written as

$$T_5 = -7.5 \left[q_{cell} + q_{CB}\right]$$

then $T_2 = T_5$. II.

Substituting $T_2 = T_5$ into equation E, T_4 may be solved as a function of T_2 as follows:

$$T_4 = 2T_2 - q_{cell}$$

which may be further reduced to

$$T_4 = -16q_{cell} - 15q_{CB} \qquad \text{III.}$$

by substituting the value of T_2 found in equation I.

Some conclusions may be drawn from equation I. and III. For T_2 to be positive, q_{CB} must be greater than q_{cell} and must be negative.

In other words, heat must be dissipated from the battery faster than it is generated.

For T_4 to be positive, q_{CB} must be $\geq 16/15\ q_{cell}$ and must be negative.

Therefore, $T_2 \geq T_4$.

By substituting various values of q_{CB}, the temperature gradient across the cell can be determined. As the centrally located cell has been selected, this will be the worst case.

q_{cell} is found directly from the duty cycle.

$$q_{Total} = \frac{9.731 \text{ watthrs.}}{\frac{447 \text{ min.}}{60 \text{ min/hr}}} = 1.3 \text{ av.}$$

$$q_{cell} = 1.3 \text{ watts} \times 3.41 \frac{\text{BTU/Hr}}{\text{watt}} = 4.42 \text{ BTU/Hr.}$$

Let $q_{CB} = -q_{cell}$

$q_{CB} = -4.42$ BTU/Hr

Then $T_2 = 0$

$T_4 = -4.42°F$

Let $q_{CB} = 17/15(-q_{cell})$

$$T_2 = -7.5 \left[4.42 - \frac{17}{15}(4.42)\right]$$

$$T_2 = -7.5 \left[4.42 - 5.0\right] = -7.5(-.48) =$$

$T_2 = 3.6°F$

$T_4 = -16q_{cell} - 15q_{CB}$

$T_4 = -16(q_{cell}) - 15\frac{17}{15}(-q_{cell})$

$T_4 = 4.42$

Let $q_{CB} = 18/15(-q_{cell})$

$T_2 = -7.5 \left[4.42 - \frac{18}{15}(-4.42)\right]$

$T_2 = -7.5 \left[4.42 - 5.3\right] = -7.5 \left[-.88\right] =$

$T_2 = 6.6$

$T_4 = -16q_{cell} - 15(\frac{18}{15} - q_{cell})$

$T_4 = 8.84$

These values are shown in Figure 15.

Two things may be learned from the foregoing study:

(1) Maximum temperature gradient with no heat sink is 57.5°F during one complete cycle.

(2) The cell temperature as experienced in a battery where sinking occurs is a direct function of the ultimate heat sink.

The values obtained in the analysis are related to the assumptions made. These are that the cell is completely insulated on three sides, and heat flows from the cell only by conduction and through the heat sink. Steady state was assumed, and the rate q_{cell} is considered uniform across the cell.

3. Thermal Analysis of a 35 AH Cell

An analysis was also made for the 35 AH cell, since we have been working with this cell and have data available to check our results.

Table IV illustrates a typical cycle and the power dissipated during such a cycle.

TABLE IV

CHARGE-DISCHARGE DUTY CYCLE

Step No.	Description	Rate(Amps)	Time(Min.)	Power(Wh)
1	Discharge	600	1	3.0
2	Charge	350	2	2.05
	Rest	0	3	0
3	Discharge	600	1	3.0
4	Charge	350	2	2.05
	Rest	0	3	0
5	Rest	0	60	0
6	Discharge	17	130	.32
7	Charge	350	5	5.12
8	Rest	0	243	0
		TOTAL	447 Min.	15.54 Wh.

$q = mC_p \Delta T$

where $q_{\text{sect } ①} = 10.1 \times 3.41 = 34.2$ BTU

$q_{\text{sect } ②} = 5.44 \times 3.41 = 18.5$ BTU

$m = 4$ lbs.

$C_p = .252$ BTU/# °F

$\Delta T_{①} = \frac{34.2}{4(.252)} = 34°F$

$\Delta T_{②} = \frac{18.5}{4(.256)} = 18.4°F$

$\Delta T_{\text{Total Cycle}} = 52.4°F$

Note that the temperature rise in the 35 AH cell is less than that of the 22 AH cell. This is directly attributable to the difference in mass.

Equations 1 - 6 are valid for this analysis. The values

of the parameters are given below:

$K = 120$ BTU/Hr ft

$W = 3.12$ in $= .26$ ft

$b = .062$ in $= .005$ ft

$L = 8.0$ in $= .67$ ft

$\therefore \frac{KLb}{2W} = .80$

& $\frac{KLb}{2L} = .115$

Equations A - F may then be rewritten:

A. $q_{cell} + .115(T_2 - T_1) + .80(T_4 - T_1)$

$q_{cell} - .915T_1 + .115T_2 + .8T_4 = 0$

B. $q_{cell} + .115T_1 - 1.030T_2 + .80T_5 = 0$

C. $q_{cell} + .115T_2 + q_{CB} = 0$

D. $q_{cell} + 1.60T_1 - 1.715T_4 + .115T_5 = 0$

E. $q_{cell} + 1.60T_2 + .115T_4 - 1.83T_5 = 0$

F. $q_{cell} + .115T_5 + q_{CB} = 0$

Equation (C) may be rewritten

$$T_2 = -8.7 \left[q_{cell} + q_{CB}\right] \qquad (C')$$

and equation (F)

$$T_5 = -8.7 \left[q_{cell} + q_{CB}\right]$$

$\therefore \quad T_2 = T_5$

Substituting $T_2 = T_5$ into (E), T_4 may be rewritten as a function of T_2

$$T_4 = 2T_2 - q_{cell}$$

This may, in turn, be revised by substituting in (C')

$$T_4 = -16q_{cell} + 15q_{CB}$$

Values for T may now be found by substituting the known value of q_{cell} and assumed values of q_{CB}.

$$q_{cell} = \frac{12.42}{447/60} \times 3.41 - 5.71 \text{ BTU/hr}$$

Let $q_{CB} = -q_{cell}$

Then $T_2 = 0$

$T_4 = -5.71°F$

Let $q_{CB} = 17/15(-q_{cell})$

$T_2 = -8.7 \quad [5.71 - 6.5] \quad = 6.90°F$

$T_4 = 5.71°F$

$q_{CB} = 18/15 (-q_{cell})$

$T_2 = -8.7(5.71 - 6.9) = 10.4°F$

$T_4 = 11.4$

These values are shown in Figure 16 and are closely related to those of Figure 15.

Of particular interest is what happens to a real cell under conditions imposed by the cycle.

A thirty-five ampere-hour cell was assembled. Thermocouples were attached to the cell at locations shown in Figure 17. The cell was then given a cycle shown in Table IV. During Section 1 (Steps 1-4), the cell rose from 77°F to 139°F (+62°F), at the terminal, and 31° at

the top of the plate. An average cell temperature rise would be quite close to theoretical value of 52°F.

The main reason for the difference between theoretical and actual temperature distribution is that the total cell impedance is the sum of several components, the largest of which is the resistance of the electrode tabs.

Thus, the assumption of q_{cell} being uniform is invalid. In addition, it would appear from the change in temperature, as shown in Tables V and VI (Cycle Data) that the assumption of steady state should be reconsidered.

It should be noted that the analysis of the unsteady state condition with non-uniform q is quite unwieldy and probably unnecessary. As may be seen from Table V, the cell temperature returns to initial conditions in two hours, and it appears from the test data that the battery will meet the imposed cycle.

TABLE V

HIGH RATE CYCLING DATA - VO-3

Time (Min.)	Comments	V	P	Temperature 4	5	6
0	Discharge at 600 A	1.38	21		77	77
0.2		1.08	21			81
0.4		1.05	23		81	
0.6		1.03	23			94
0.8		1.02	23		86	100
1.0		1.02	23			104
	Charge at 350 A					
1.5		1.48	23		93	107
2.0		1.52	24	83	93	112
2.5		1.56	25	86	95	116
3.0		1.78	47	88	96	116
4.0	Rest			90	97	106
5.0				90	96	106
6.0						
	Discharge at 600 A					
6.2		1.07	44			108
6.4		1.05	45		97	
6.6		1.35	45			118
6.8		1.02	45		105	
7.0		1.02	45			125

TABLE V continued

Time (Min.)	Comments	V	P	Temperature 4	5	6
	charge at 350 A					
7.5		1.48	45	98	108	132
8.0		1.52	46	98	108	135
8.5		1.56	48	99	108	136
9.0		1.80	78			139
10	Rest	1.38	87			
11		1.36	87			
12		1.36	86			
	Place on open circuit for 2 hours			81	81	81

TABLE VI

"C" RATE DISCHARGE - VO-35

Time (Min.)		V	P
	OCV & P	1.32	60
1		1.28	60
10		1.25	58
15		1.24	58
20		1.24	57
25		1.23	57
30		1.23	57
37		1.22	56
40		1.22	56
45		1.22	56
50		1.21	55
51		1.21	55
52		1.21	55
53		1.20	55
54		1.20	55
55		1.20	54
56		1.20	54
57		1.20	54
58		1.19	54
59		1.19	54
60		1.19	54
61		1.18	54
62		1.17	54
63		1.16	54
64		1.14	53
65		1.05	
65.2		1.0	

IV. CHARGE CONTROL-CHARGE CONDITIONING SYSTEM

A schematic diagram of the parallel chopper system is shown in Figure 18. It consists of five identical power systems connected in parallel. These sections are operated sequentially, thereby reducing the aircraft bus ripple and battery ripple to a tolerable level, and eliminating the need for external filtering. A description of the operation of one of the power sections is given below:

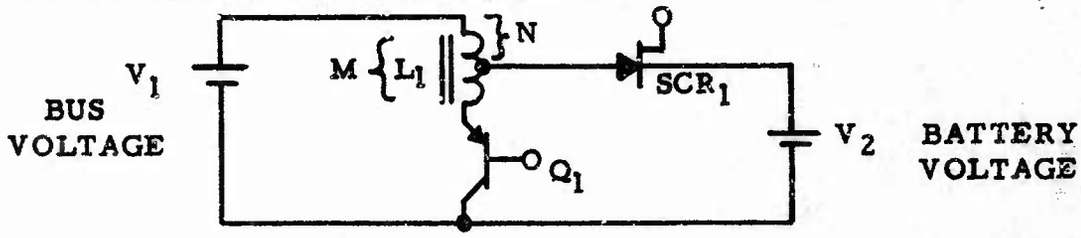

Above is a schematic diagram of one power section of the parallel chopper. L_1, Q_1 and SCR_1 make up an elementary flyback booster. If Q_1 is periodically turned on, the current flowing Q_1 will store energy in L_1. When Q_1 is turned off, this stored energy will be added to the aircraft bus energy. This will cause current to flow through SCR_1 into the battery.

The boost voltage supplied by L_1 is

$$V_{boost} = V_1 \frac{N}{M} \frac{t_{on}}{t_{off}} \qquad \text{(Eq. 1)}$$

where:

N = number of turns of upper winding of L_1

M = total number of turns of L_1

t_{on} = time Q_1 is on

t_{off} = time Q_1 is off

This equation shows that for a given tap ratio ($\frac{N}{M}$) and bus voltage

(V_1), the boost voltage can be varied by changing the ratio of the "on" time to the "off" time of Q_1.

The magnitude of current delivered to the battery can be calculated quite readily, since the energy stored in the inductor prior to Q_1 being turned off must be equal to the stored energy after Q_1 is turned off (conservation of flux). The resulting current is

$$I_b \text{ (max.)} = \frac{M}{N} I_{Q_1} \text{ (max.)} \qquad \text{(Eq. 2)}$$

This current flowing in the battery will decrease from its maximum value as the stored energy in the inductor is supplied to the battery. If the value of inductance is large compared to the off time of Q_1, this decrease in current will be negligible. Thus, the use of a tapped inductor permits large values of current to be delivered to the battery while Q_1 is required to handle only a fraction of this current.

It would seem that the value of current flowing through Q_1 could be made as small as desired by decreasing the ratio of $\frac{N}{M}$. However, as can be seen by inspecting equation 1, a decrease in the ratio of $\frac{N}{M}$ will cause an equal decrease in the ratio of the off time to the on time of Q_1 for any given value of V_{boost} and V_1. This will tend to decrease the average current delivered to the battery. By combining equations 1 and 2, the following equation for the average current delivered to the battery may be derived.

$$I_b\,(av.) = \frac{I_{Q_1}\,(max.)}{\frac{N}{M} + \frac{V_{boost}}{V_1}} \qquad \text{(Eq. 3)}$$

Equation 3 shows that there is an upper limit of average current which may be delivered to the battery which is equal to $\frac{I_{Q_1\,(max)}\,V_1}{V_{boost}}$. This will occur when the ratio of $\frac{N}{M}$ is zero. Thus, equation 3 shows that the average current delivered to the battery will increase toward a maximum of $\frac{I_{Q_1}\,(max)\,V_1}{V_{boost}}$ as the ratio $\frac{N}{M}$ is decreased from a value of one (corresponding to an untapped inductor) to a value of zero (corresponding to a tapped inductor with an infinite tap ratio).

A consideration which places a lower limit on the ratio of $\frac{N}{M}$ is that the maximum reverse voltage which the collector junction of Q_1 must handle is given by

$$V_{RQ1}\,(max) = \frac{M}{N}\;V_{boost} + V_2$$

assuming the following values of voltage:

$V_{RQ_1}\,(max) = 70$ volts

$V_{boost} = 8$ volts

$V_2 = 32$ volts

This sets the minimum value of $\frac{N}{M}$ at approximately one-fourth.

The minimum value of V_1, as defined in the Work Statement, is 26 volts. This sets the ratio of the average battery current to the maximum average current (corresponding to $\frac{N}{M} = 0$) at approximately 0.55. Any substantial increase in this ratio would

require the use of a much more costly transistor for Q_1. Referring once again to Figure 18, five parallel units are used, with each unit delivering approximately 80 amperes, average current to the battery.

As can be seen from Figure 18, the details of the protection and control circuits have been omitted. There are two reasons for this. First, the operations which the control circuits and protection circuits must perform can be determined only after a laboratory study of the characteristics of paralleling individual power sections. Second, an accurate estimation of the size and weight of the control and protection circuits can be made based upon our experience with similar systems.

The following table gives a projected parts list:

TABLE VII

PROJECTED PARTS LIST OF PARALLEL CHOPPER

Component	Value or Part Number	Manufacturer
$Q_1 - Q_5$	MP-501	Motorola
$CR_1 - CR_5$	C55F	General Electric
$L_1 - L_5$	160 uh, 160A, 5KHZ	Custom Made
K_1	AN-3381-2	Cutler-Hammer

The total weight of this unit is 14.3 pounds. The weight breakdown is shown in the following table.

TABLE VIII

ESTIMATED WEIGHT BREAKDOWN OF PARALLEL CHOPPER

Component	Weight
Transistors Q_1 - Q_5	0.25 lbs.
SCR's CR_1 - CR_5	1.25 lbs
Inductors L_1 - L_5	5.00 lbs.
Discharge Relay - K_1	2.30 lbs.
Control Circuits	0.50 lbs.
Napthalene	2.00 lbs.
Brackets and Structure	3.00 lbs.

The power losses during charge are shown in the following table:

TABLE IX

ESTIMATED POWER LOSSES OF PARALLEL CHOPPER

Component	Power Loss
OUTPUT SCR's	
1.2 volts x 350 amperes	420 watts
TRANSISTORS	
Drive Losses 0.6 volts x 11 amps	6.6 watts
Saturation Losses 0.35 volts x 110 amps	38.5 watts
Switching Losses	30.0 watts
INDUCTORS	
Copper Losses	100 watts
Core Loss	75 watts
CONTROL CIRCUITS	20 watts

The total power dissipated during charge is 690 watts. Figure 19 is a sketch of the proposed arrangement of circuit components.

To date three charge control-charge conditioning systems have been designed. They are the inverter phase control, SCR phase control, and the parallel chopper systems. The major difference between these systems is the method used to condition the aircraft bus to the optimum requirements of the battery. Table X contains the calculated size, weight and power loss of each system.

TABLE X

COMPARISON OF CHARGE CONDITIONING SYSTEMS

System	Size	Weight	Power Loss
Inverter Phase Control	236 $in.^3$	13.8 lbs.	677 watts
SCR Phase Control	186 $in.^3$	13.7 lbs.	685 watts
Parallel Chopper	209 $in.^3$	14.3 lbs.	690 watts

The SCR phase control system occupies 21% and 11% less volume than the inverter phase control and parallel chopper systems, respectively. The extent of this advantage of the SCR phase control system might not be realized in practice, since the calculations upon which the size of each system is based could be in error by about ±5%.

The calculated weight and power loss for each system differ by such insignificant amounts that a value judgment based upon them

would be meaningless.

The inverter phase control system has an inherent disadvantage because a contactor must be employed in order to terminate battery charging current. This contactor must interrupt a current of approximately 350 amperes. This will produce arcing at the contacts, and would probably limit the maintenance-free life of this system. Arc suppression techniques, such as placing a capacitor across the contacts, would either not be effective enough, or would occupy too much volume.

Arcing will not result at the contacts of the discharge contactor, contained in each system, since it will open only after current has been terminated by other switches in the aircraft power system.

Because of the arcing problem, and the larger volume of the inverter phase control system, we do not feel that its development will produce a system as effective as the SCR phase control and parallel chopper systems.

V. CONCLUSIONS

The behavior of the 35 AH prototype cell has been shown to be satisfactory on high rate discharge at temperatures as low as -30°F. The high rate charge characteristics are satisfactory at temperatures of 20°F and above. At temperatures below 20°F hydrogen gassing occurs during the initial portion of the charge.

The Adhydrode has given good response to oxygen pressure buildup in the cell at all temperatures. Its signal is oxygen pressure and temperature dependent.

The $Cd/Cd(OH)_2$ coulometer was found to give a premature signal at low temperature. In addition, its input and output signals differed for different rates. These characteristics could cause an imbalance between it and the battery preventing the battery from fully charging or causing the battery to overcharge.

Test results on the first 22 AH prototype cell indicated that the cell has good high rate charge and discharge capability at room temperature.

A comparison among the three methods to condition the aircraft bus to the requirements of the battery indicate that the SCR phase control and the parallel chopper are preferable. Of these two, the latter is inherently simpler.

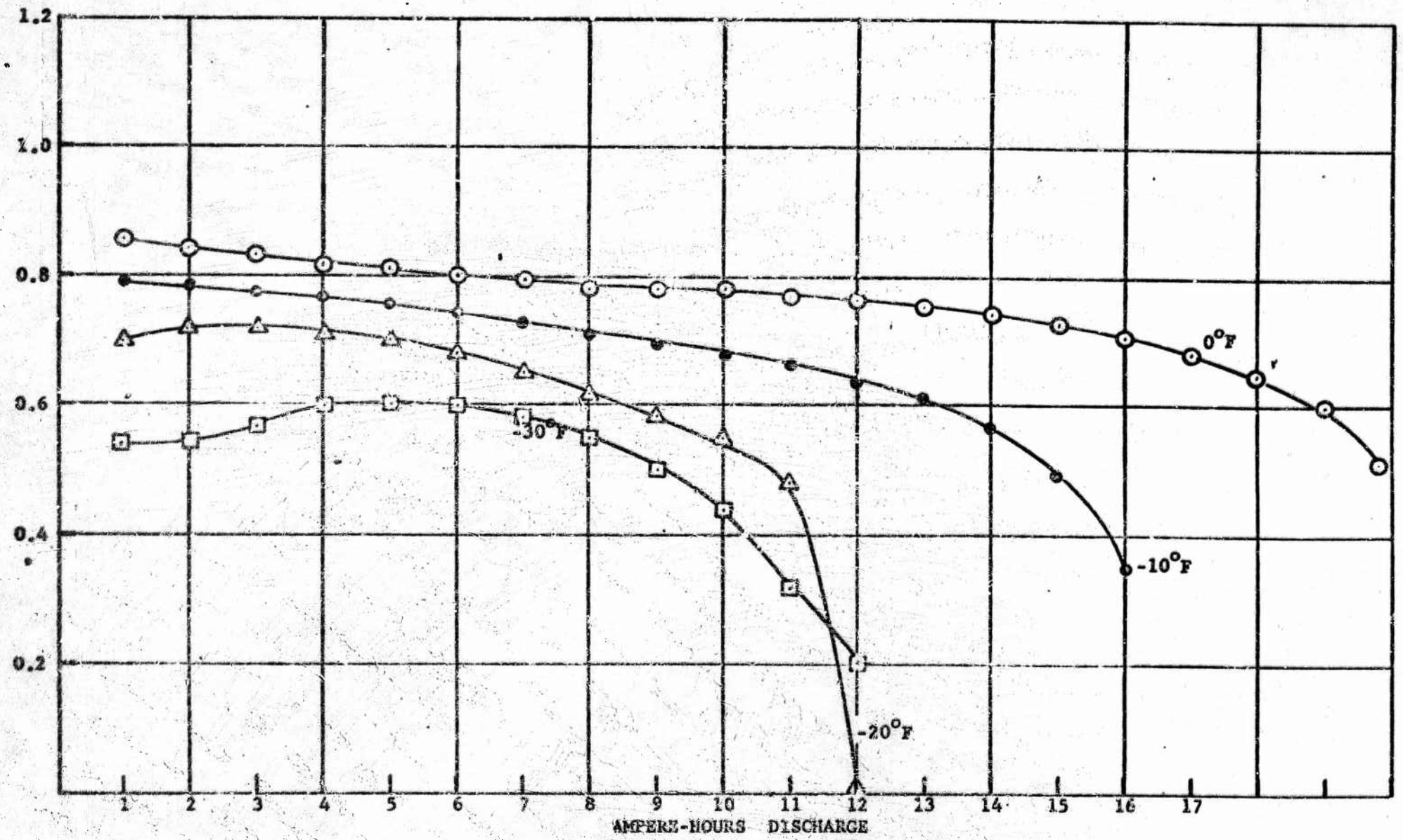

FIGURE 1. VOLTAGE Vs. TIME - 600 AMPERE DISCHARGE AT VARIOUS TEMP.
35 AH CELL

M3593

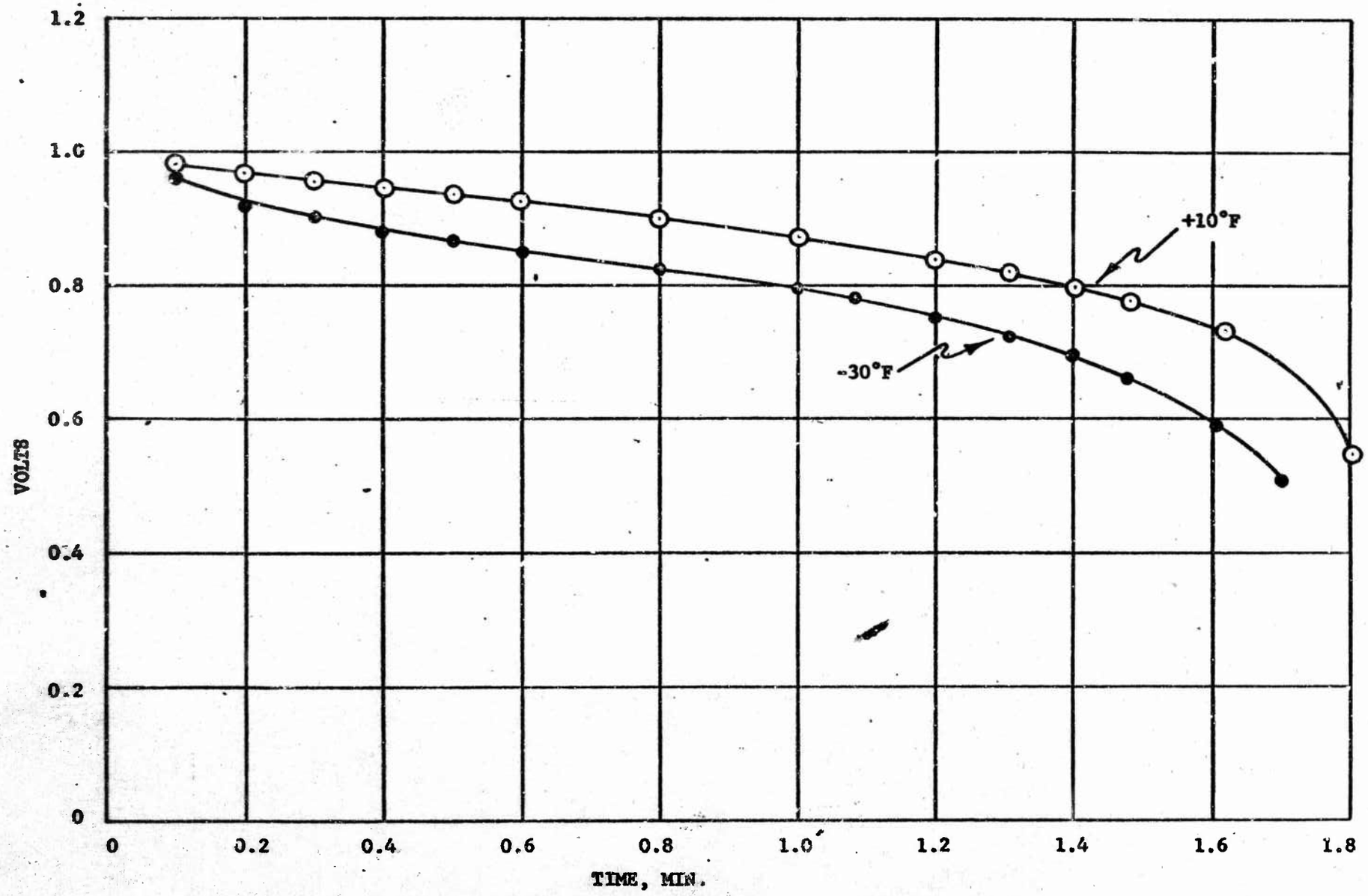

FIGURE 2. 600 AMPERE DISCHARGE FOLLOWING 350 AMPERE CHARGE
35 AH CELL

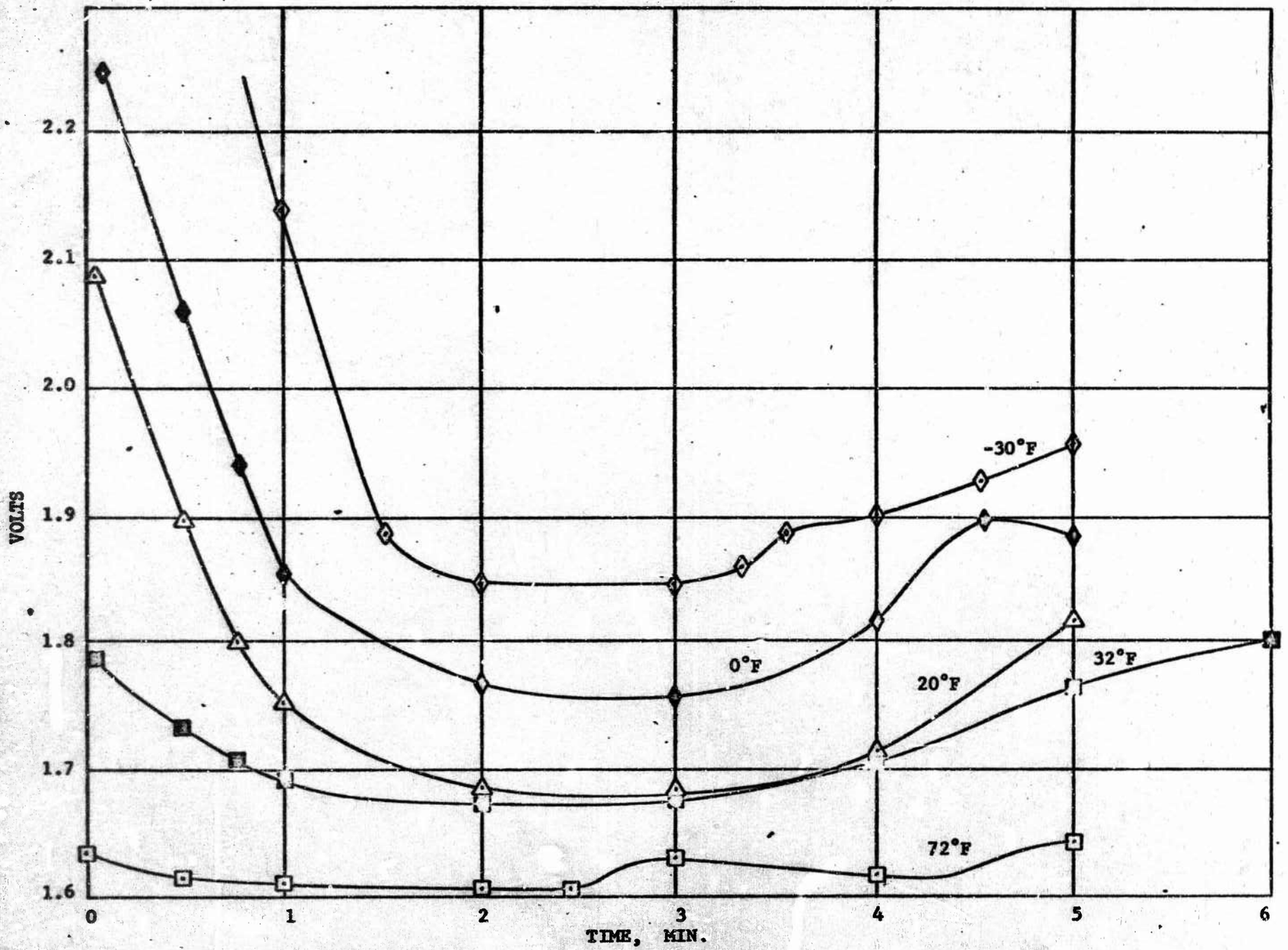

FIGURE 3. 350 AMPERE CHARGE AT VARIOUS TEMPERATURES
35 AH CELL

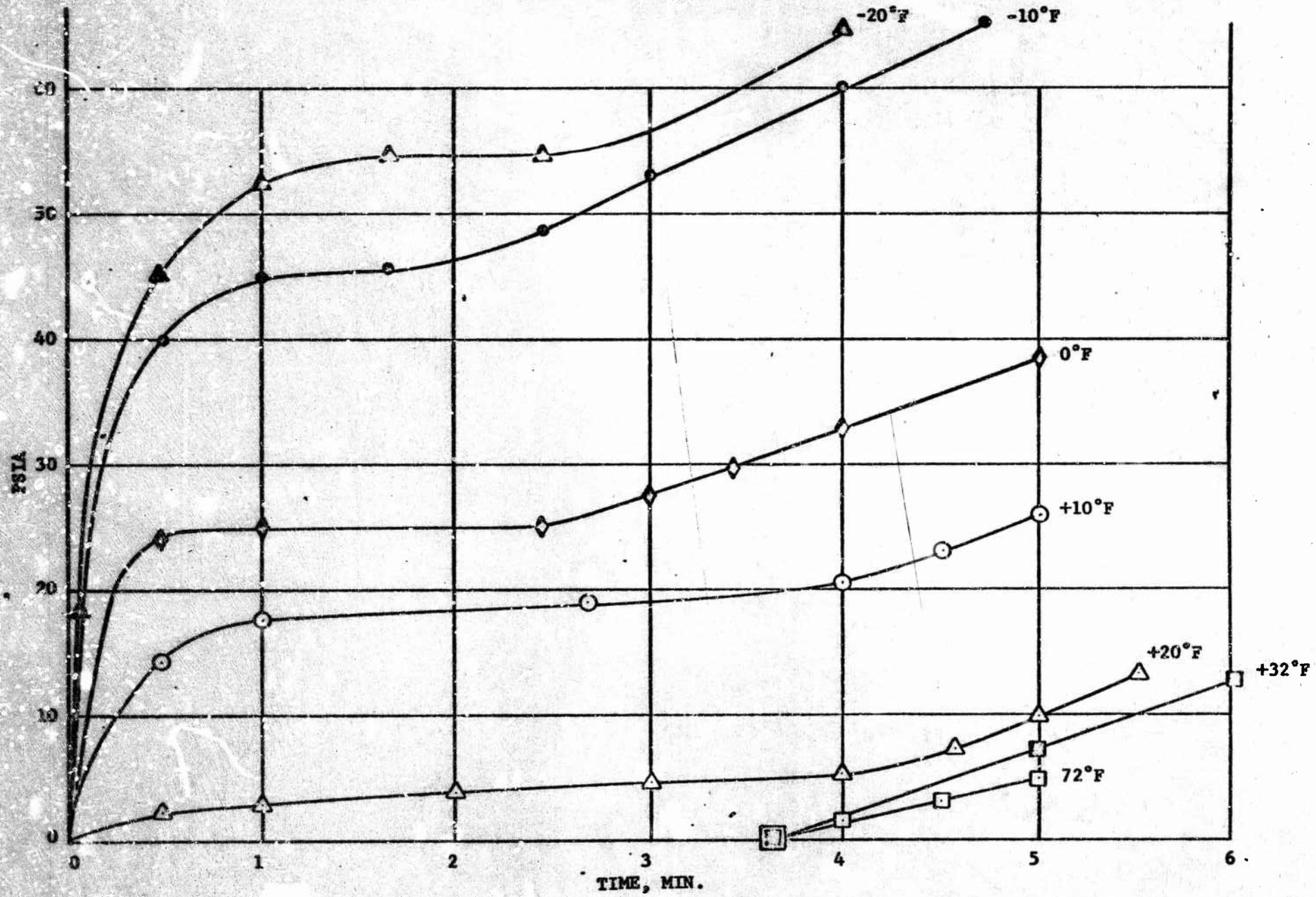

FIGURE 4. PRESSURE VERSUS TIME ON 350 AMPERE CHARGE
35 AH CELL

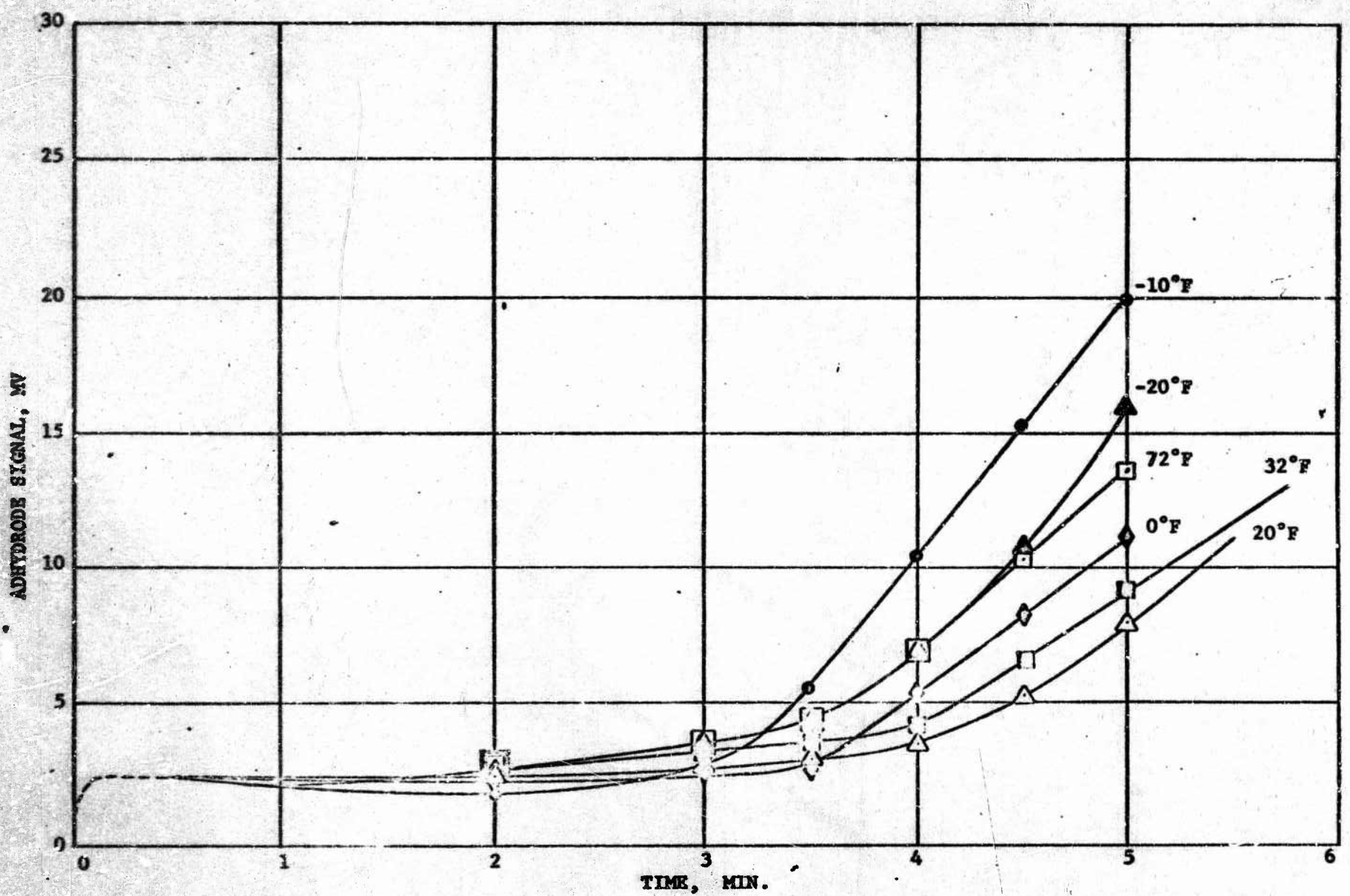

FIGURE 5. ADHYDRODE SIGNAL VERSUS TIME, 350 AMPERE CHARGE
35 AH CELL

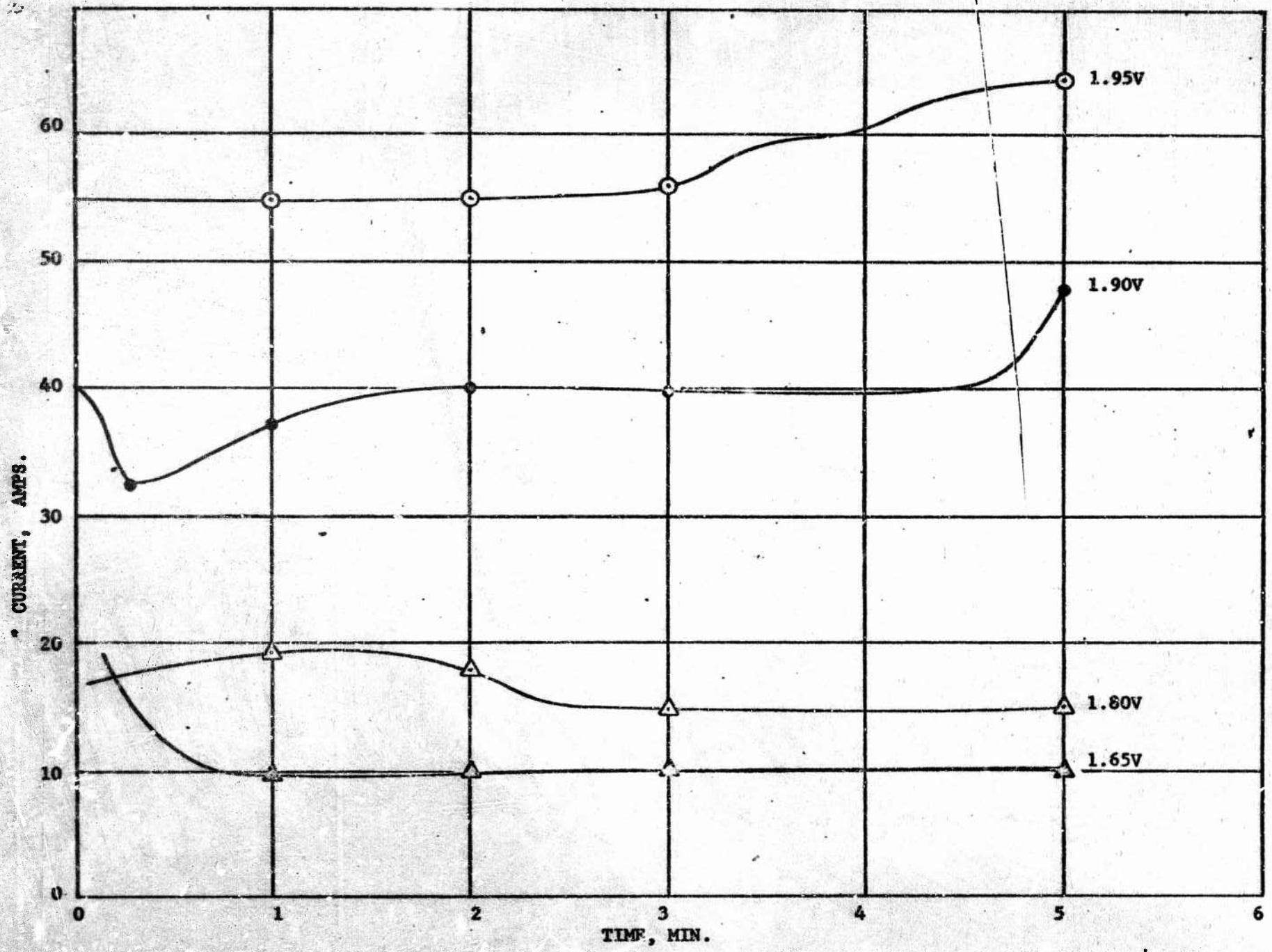

FIGURE 6. CONSTANT POTENTIAL CHARGE AT -30°F, 35 AH CELL

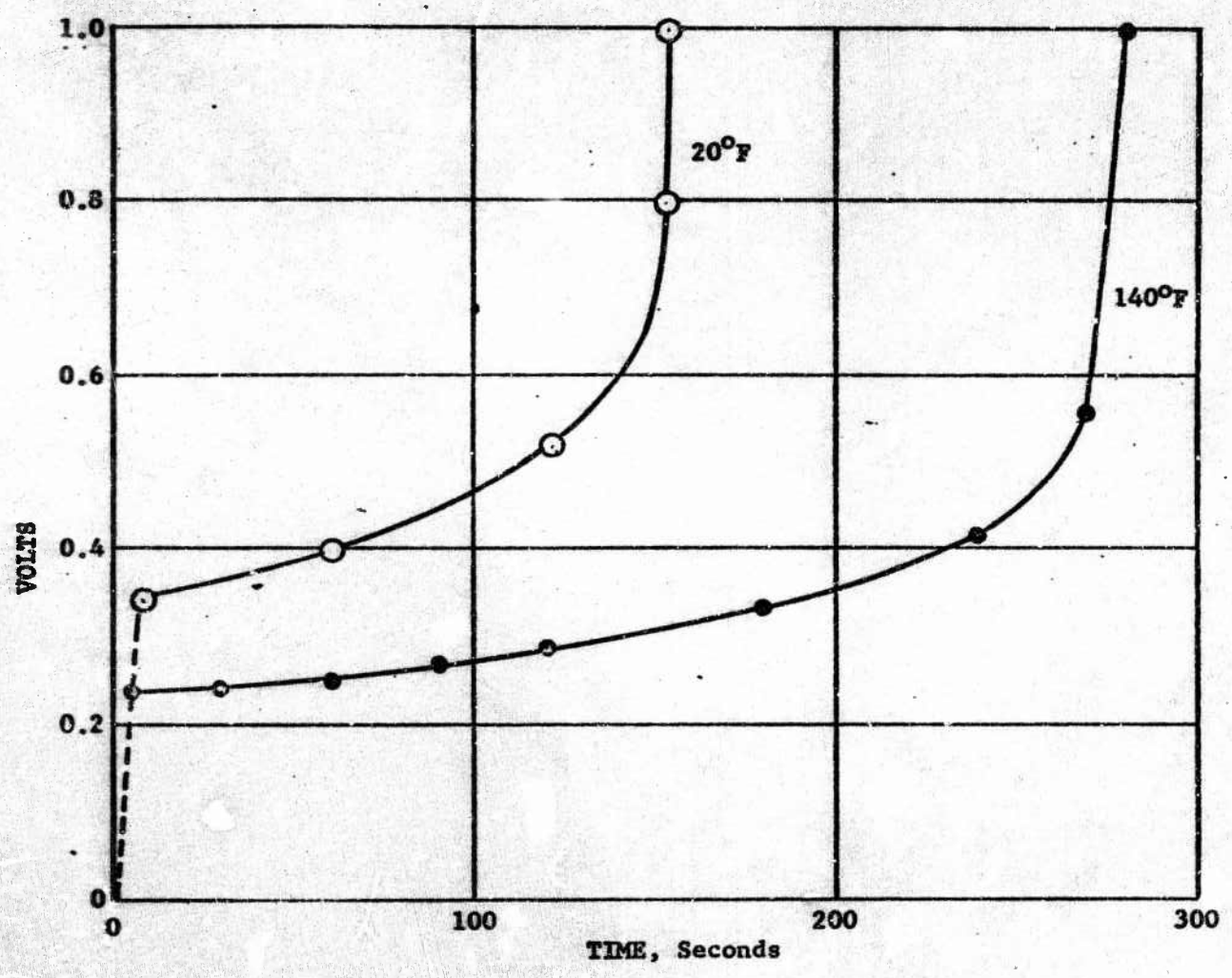

FIGURE 7. COULOMETER VOLTAGE DURING 350 AMPERE CHARGE

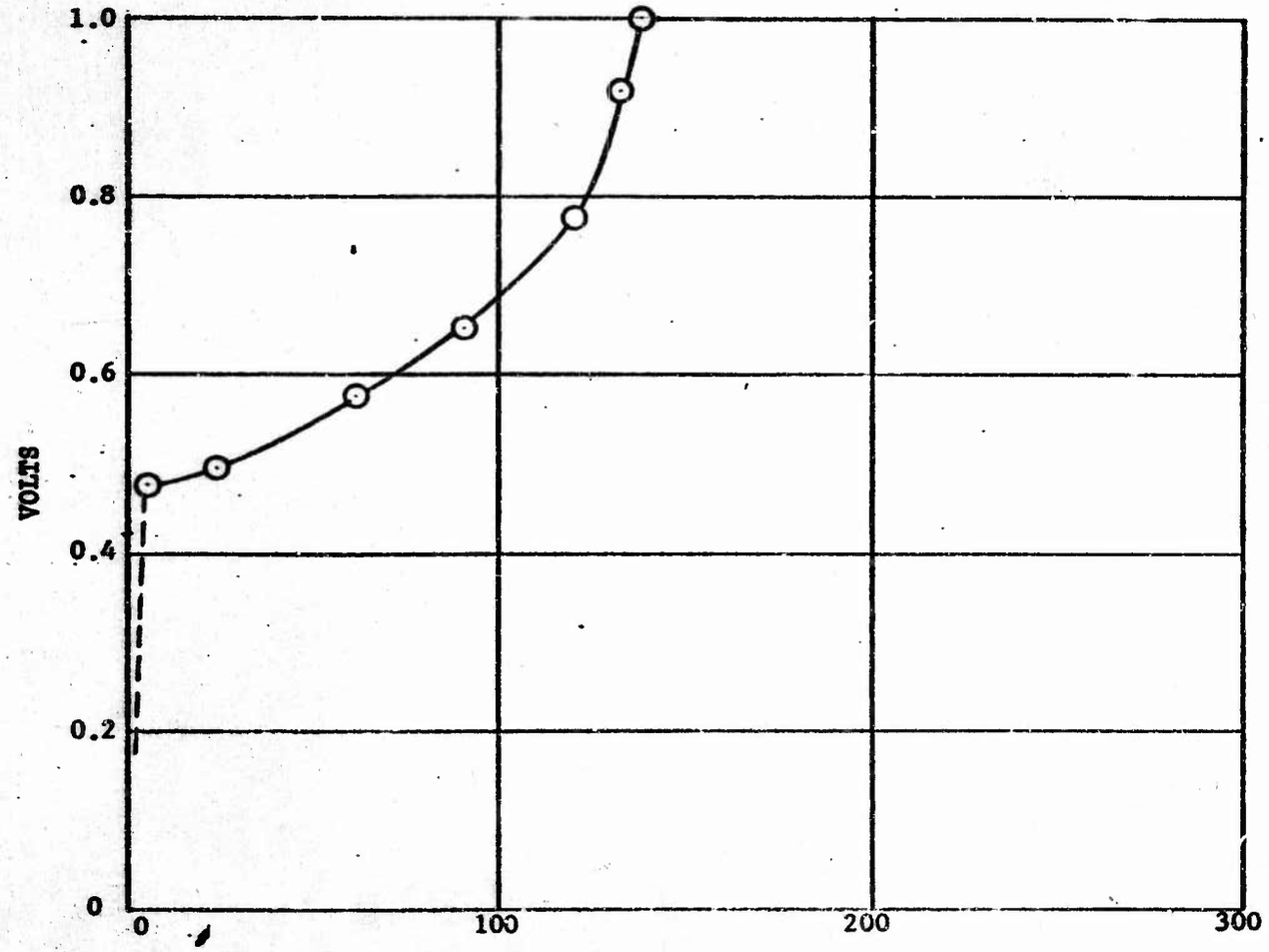

FIGURE 8. COULOMETER VOLTAGE DURING 600 AMPERE DISCHARGE AT 140°F

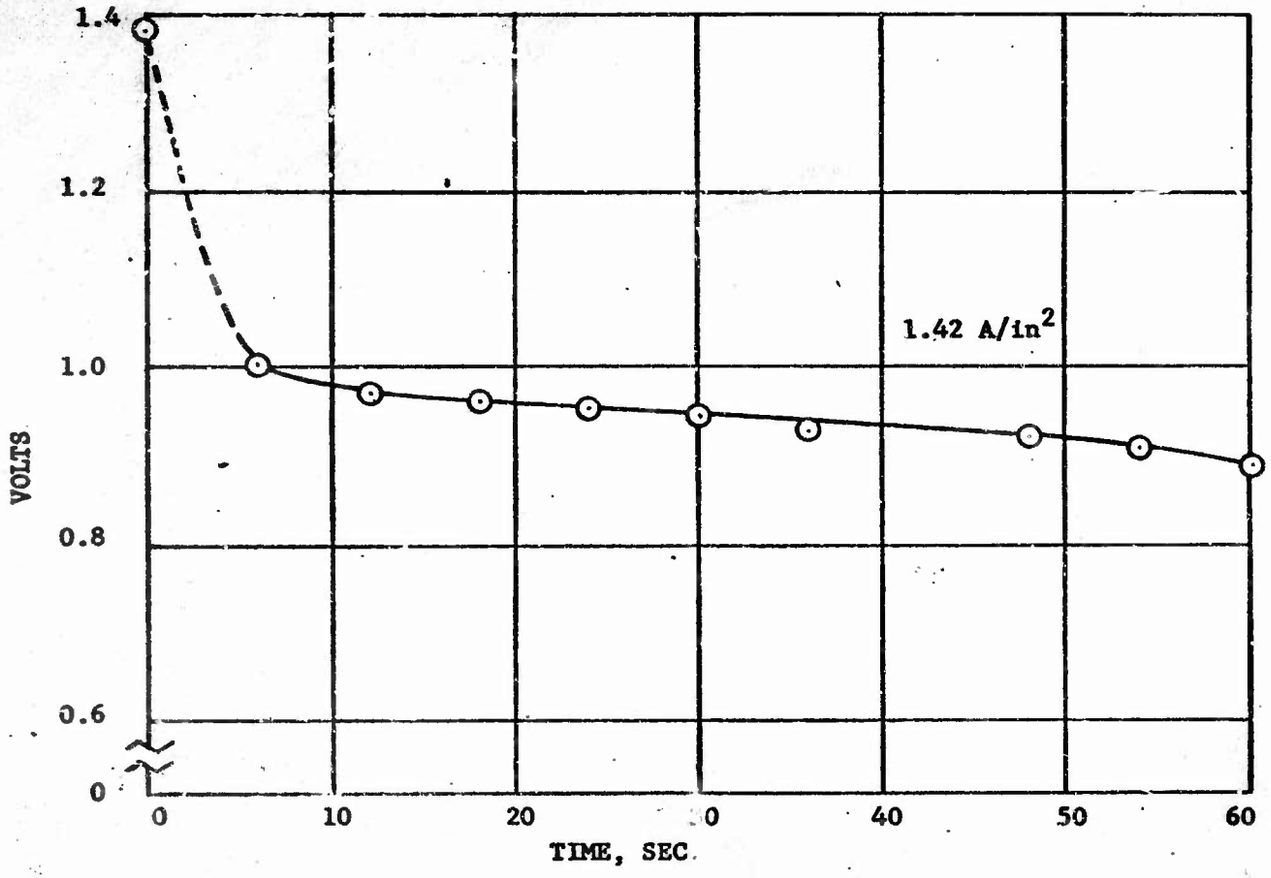

FIGURE 9. 600 AMPERE DISCHARGE AT ROOM TEMPERATURE 22 AH LP-1
CHARGE AT 22 AMPERES 66 MIN. AT ROOM TEMPERATURE

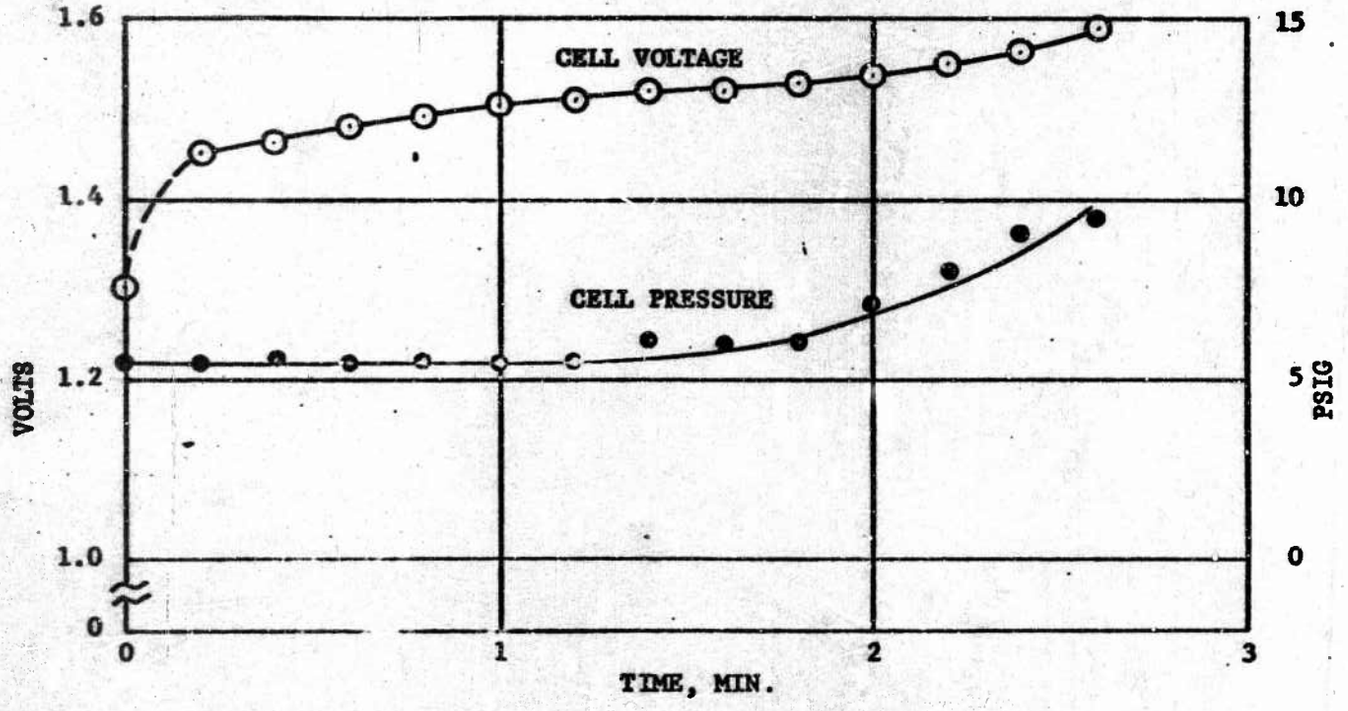

FIGURE 10. 220 AMPERE CHARGE AT ROOM TEMPERATURE 22 AH LP-1
FOLLOWING 600 AMPERE DISCHARGE

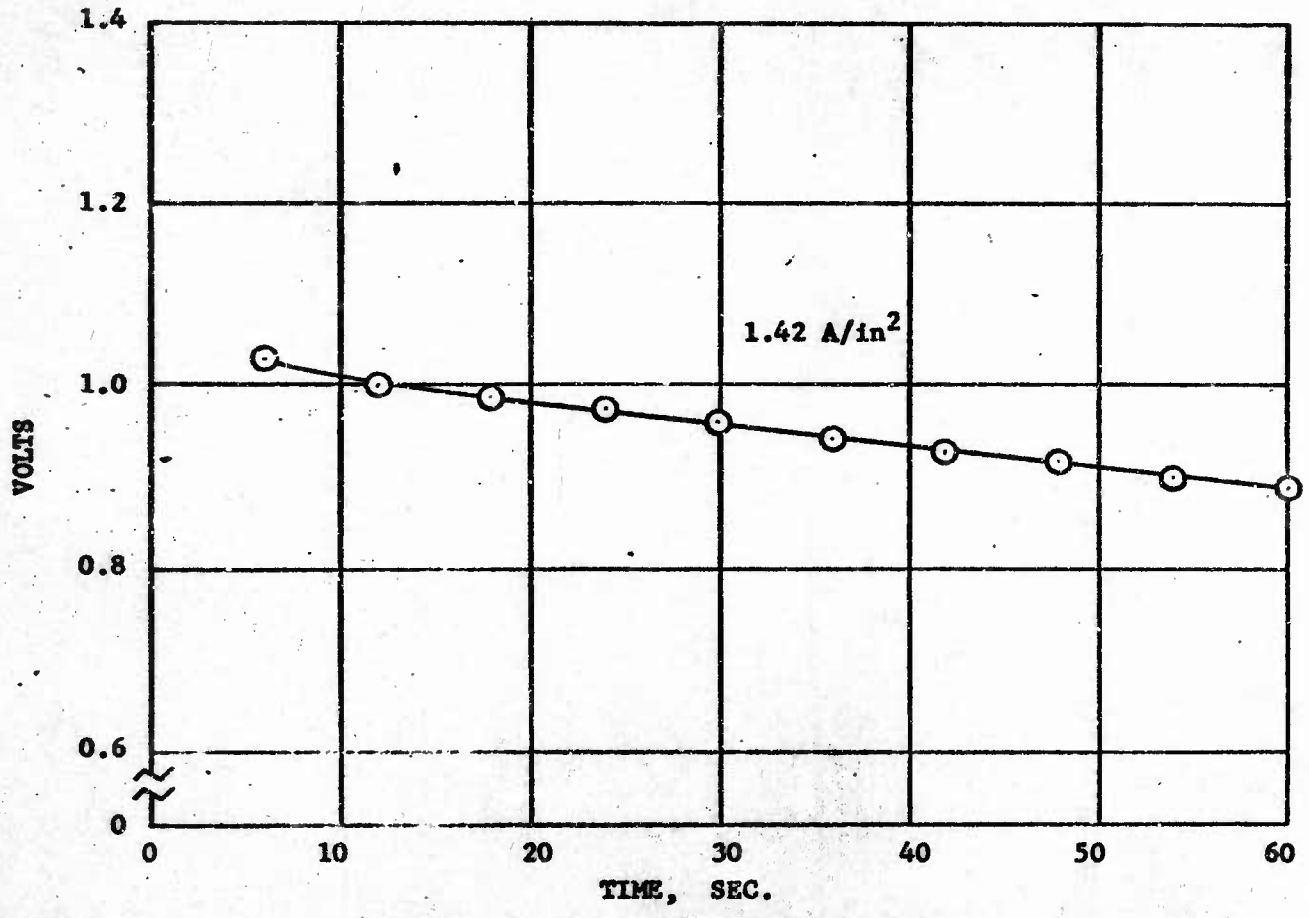

FIGURE 11. 600 AMPERE DISCHARGE AT ROOM TEMPERATURE 22 AH LP-1 FOLLOWING 220 AMPERE CHARGE

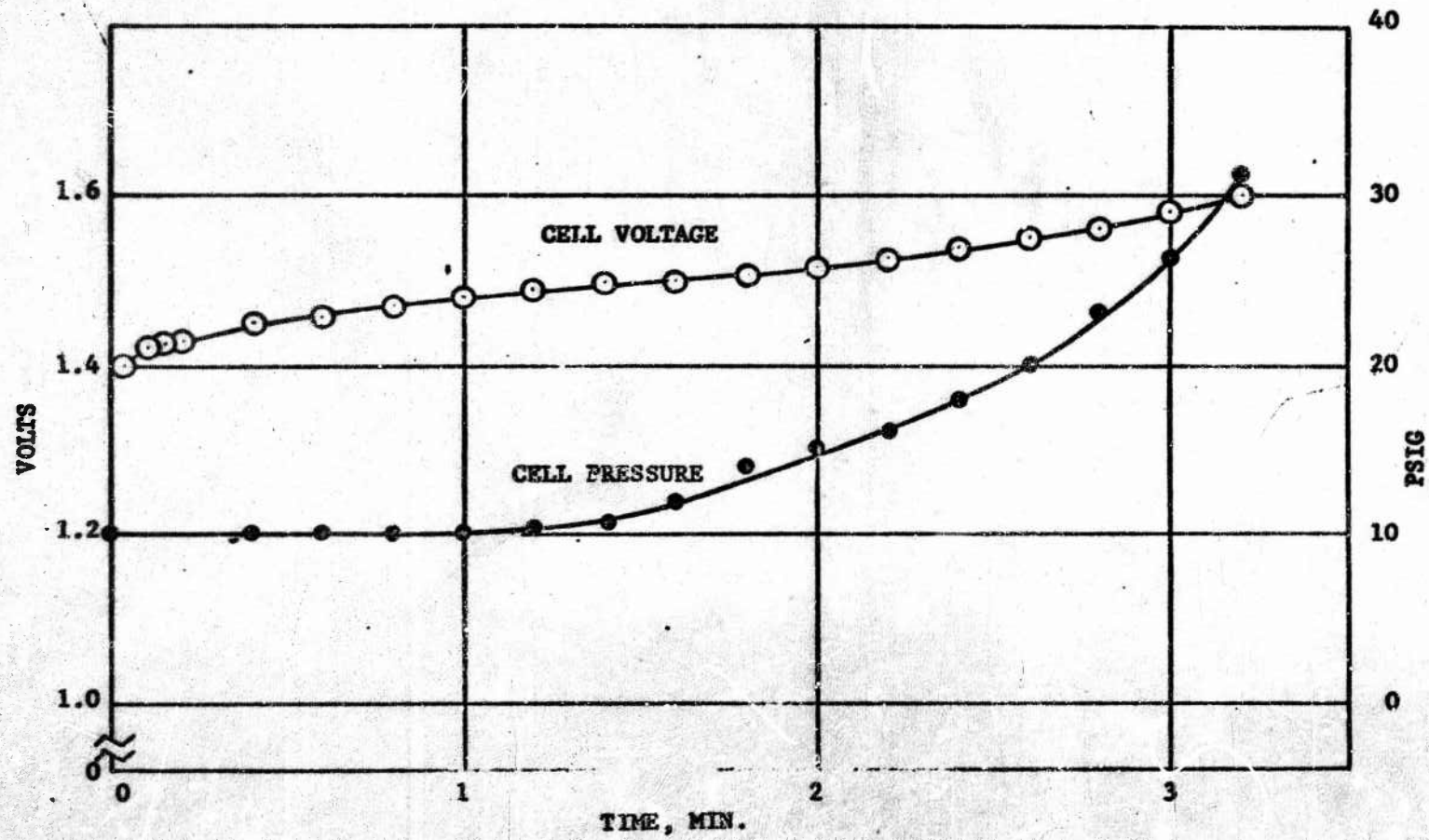

FIGURE 12. 220 AMPERE CHARGE AT ROOM TEMPERATURE 22 AH LP-1 FOLLOWING 600 AMPERE DISCHARGE

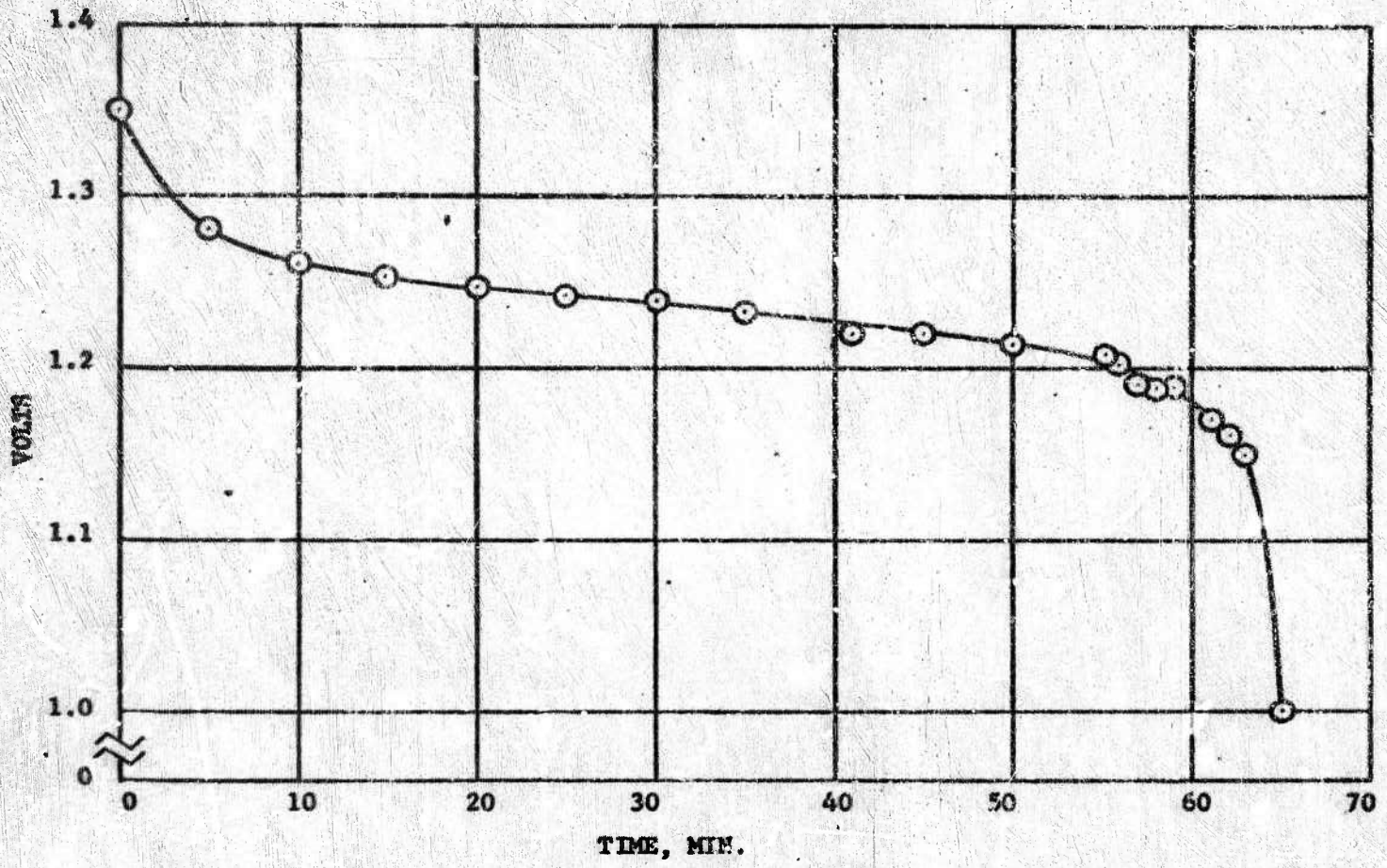

FIGURE 13. 22 AMPERE DISCHARGE AT ROOM TEMPERATURE 22 AH LP-1
FOLLOWING 220 AMPERE CHARGE

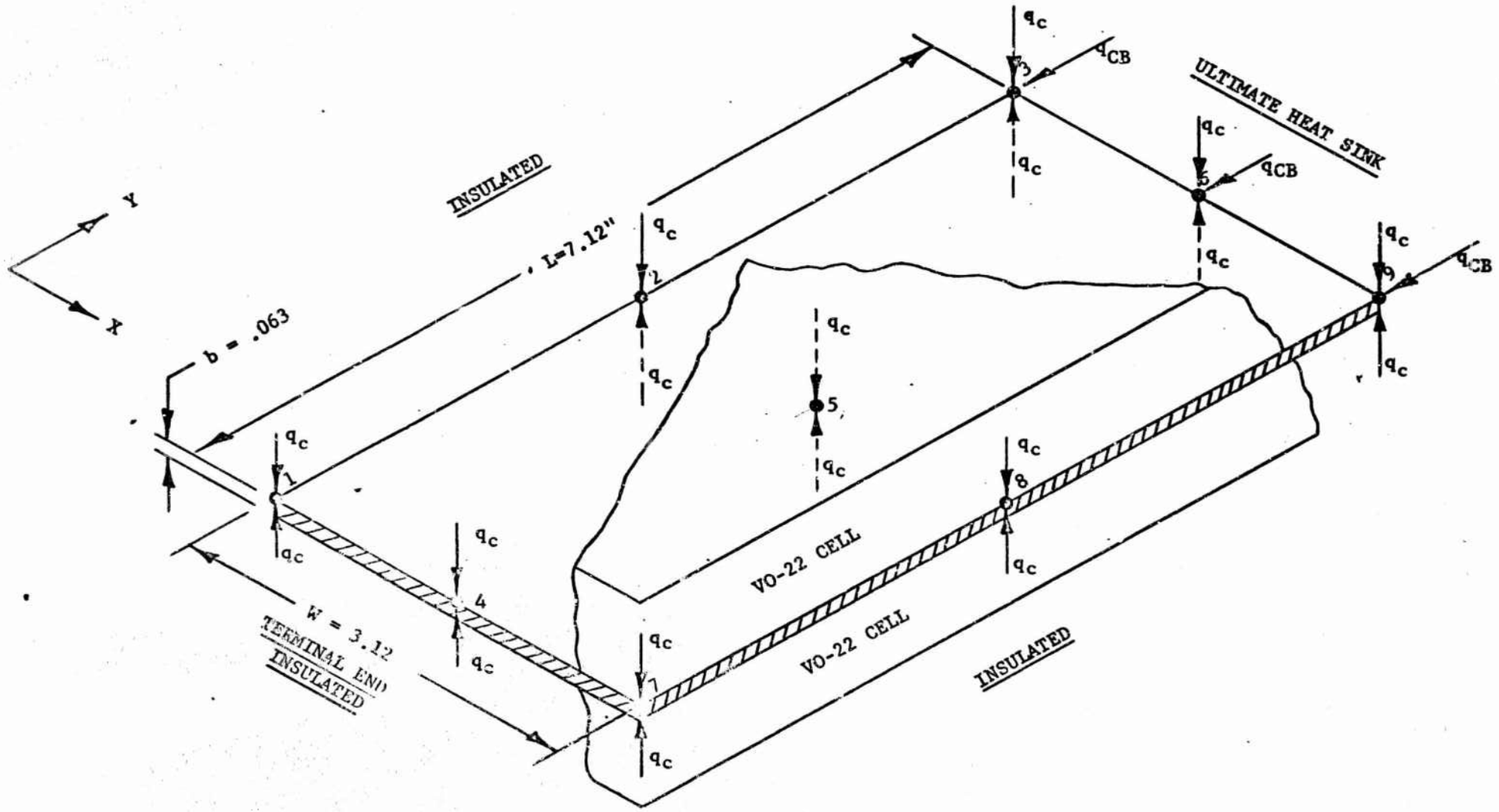

q_c = $\frac{1}{2} q_{cell} \ldots q_{cell}$ Flows into each nodal point

q_{CB} = Heat conducted from the ultimate heat sink

FIGURE 14. HEAT SINK FIN

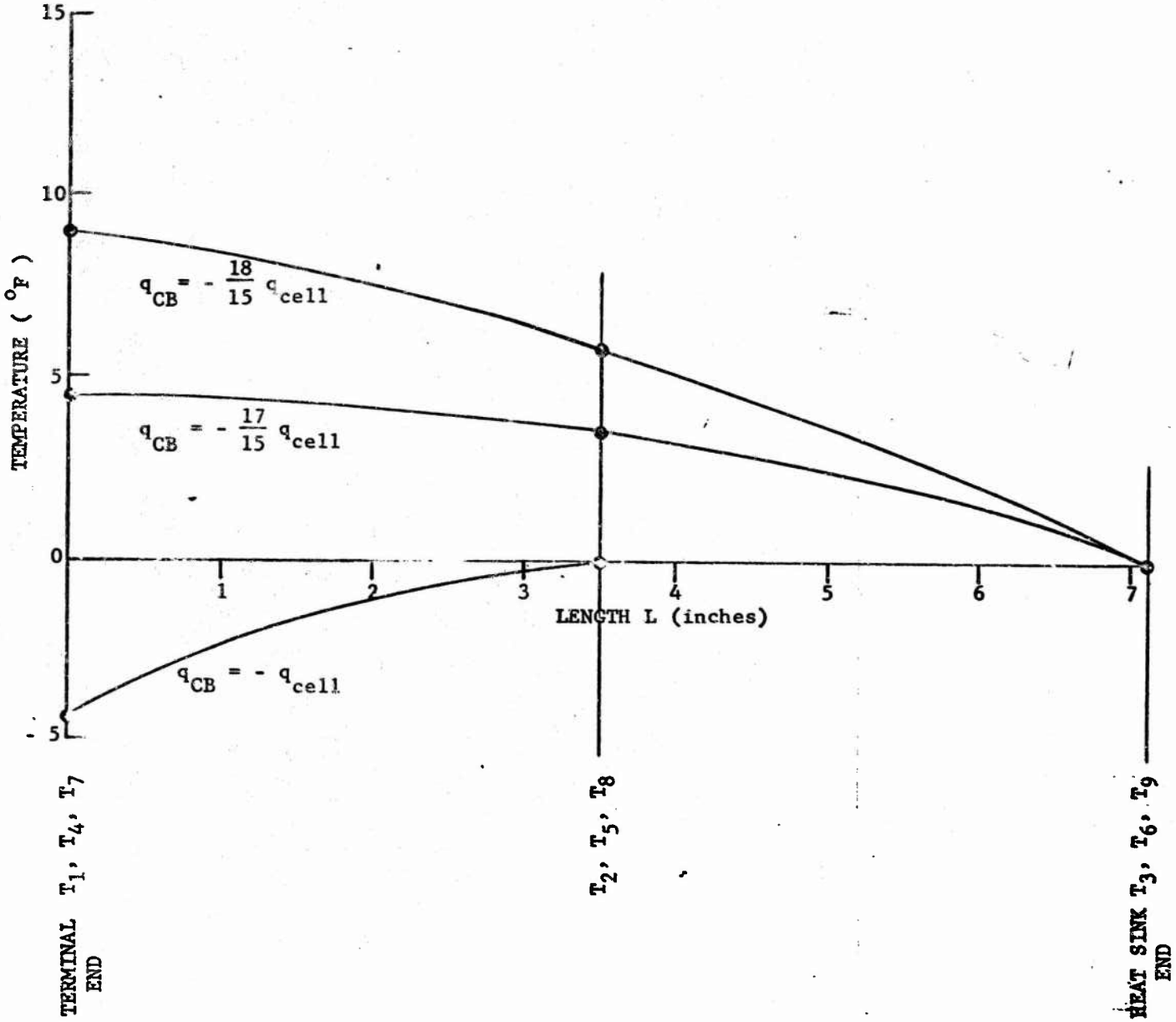

FIGURE 15. THERMAL GRADIENT ACROSS 22 AMPERE-HOUR CELL

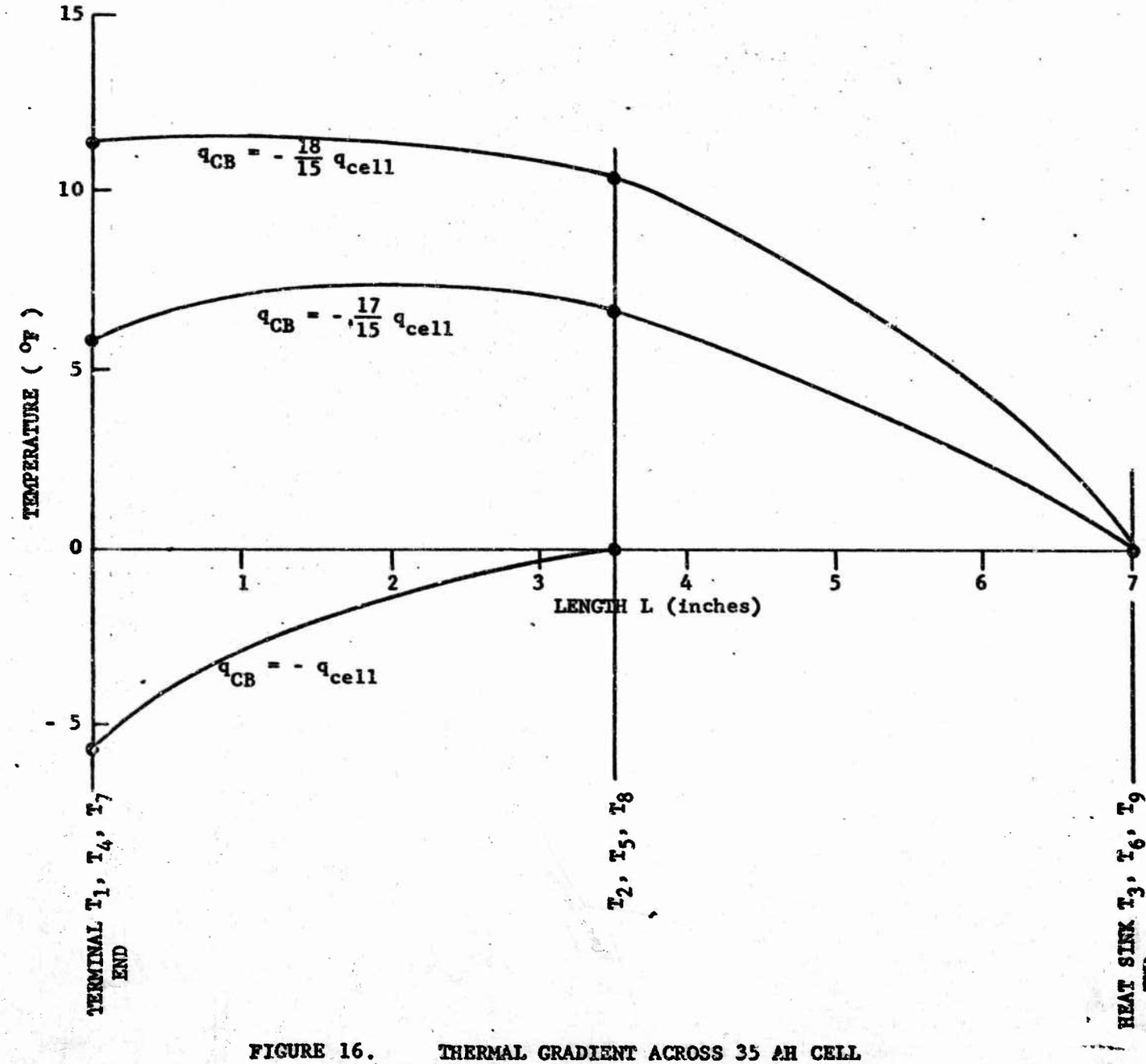

FIGURE 16. THERMAL GRADIENT ACROSS 35 AH CELL

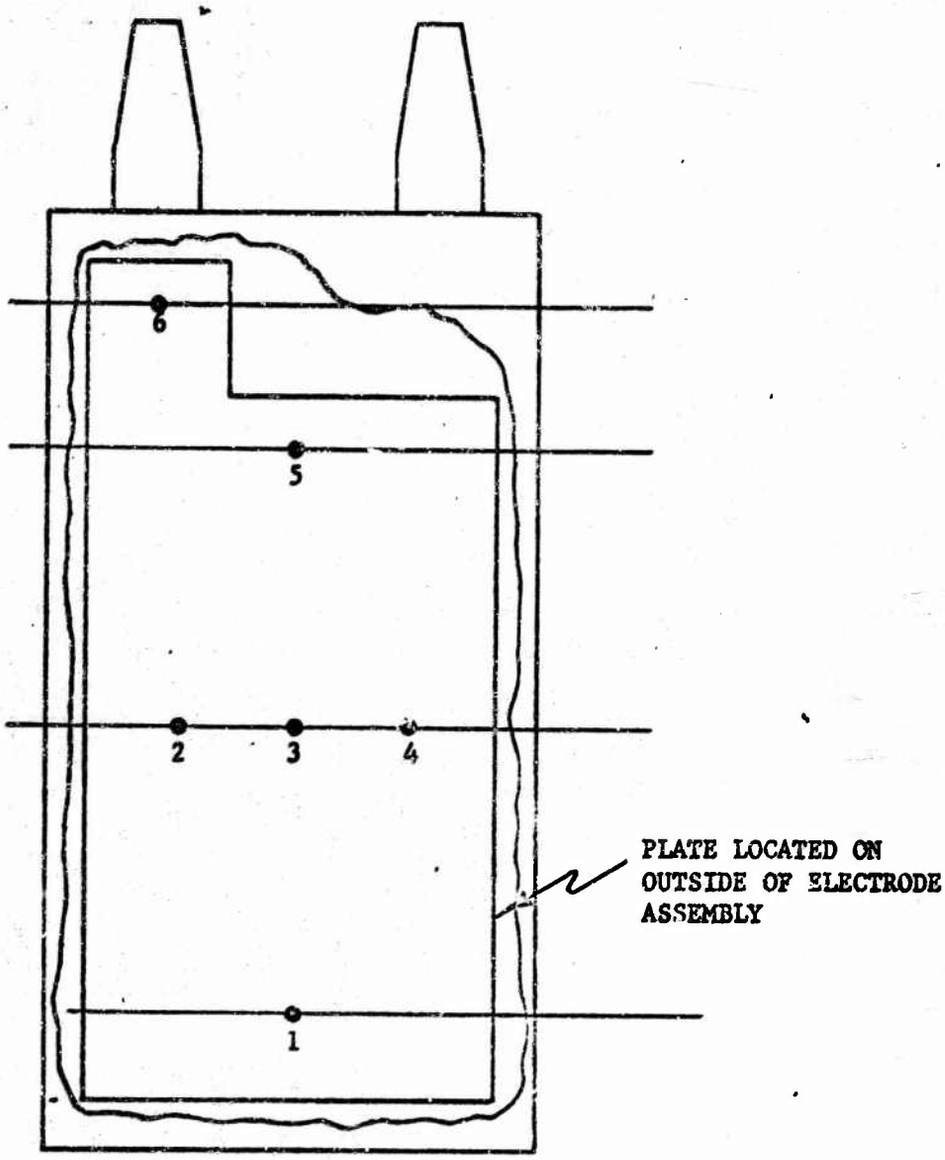

FIGURE 17. THERMOCOUPLE LOCATION

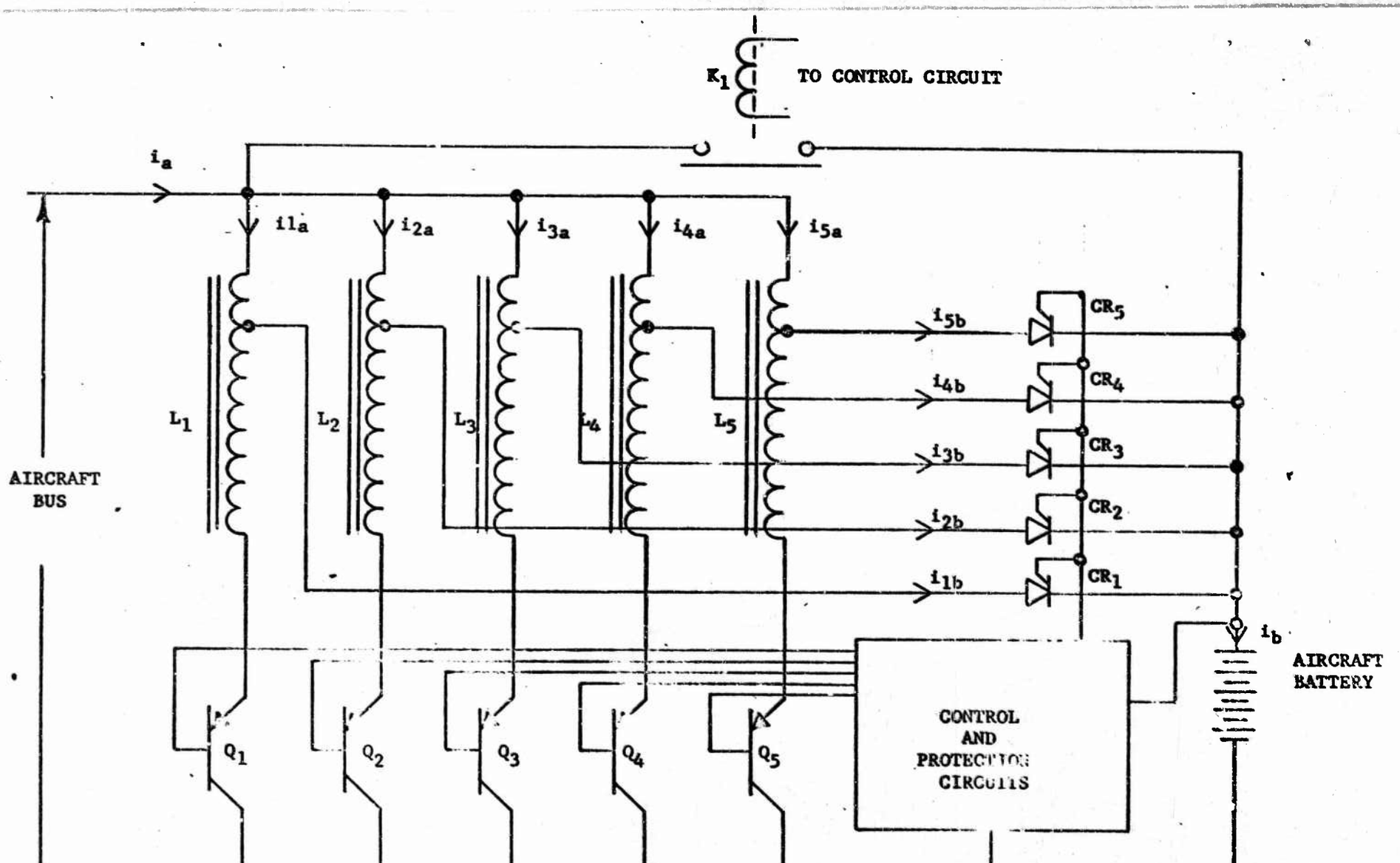

FIGURE 18. SCHEMATIC DIAGRAM OF PARALLEL CHOPPER SYSTEM

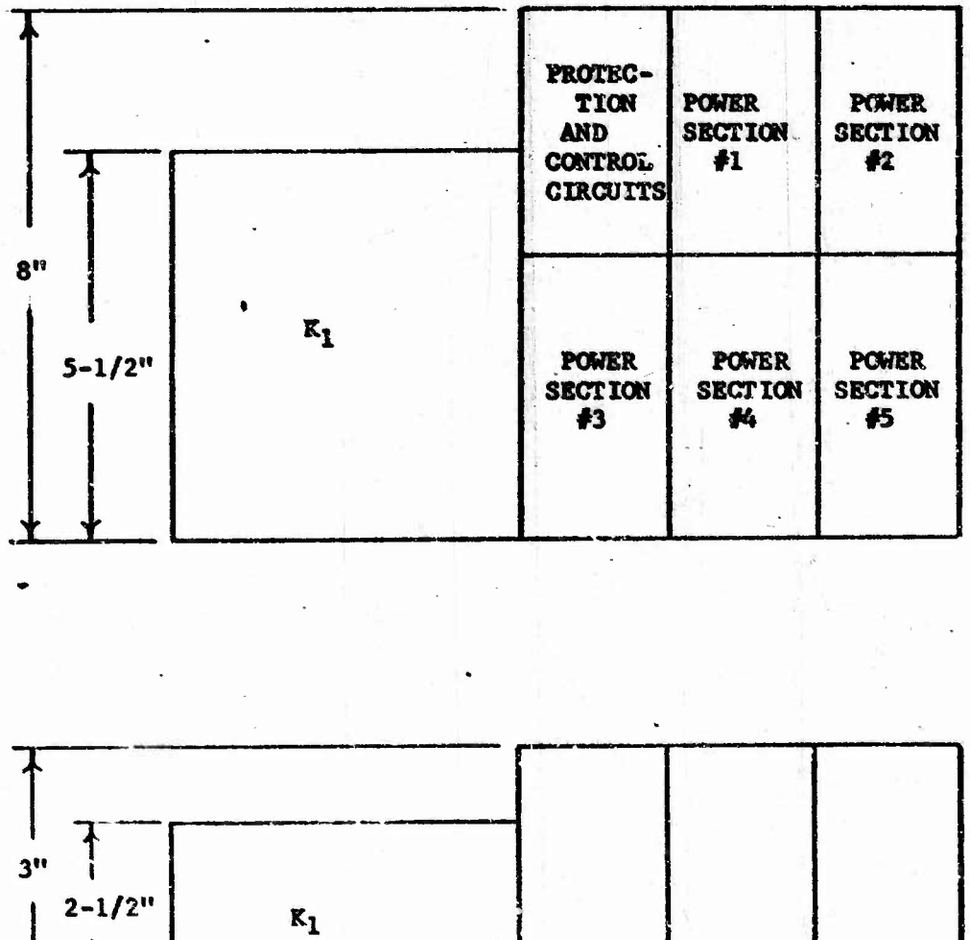

FIGURE 19. SKETCH OF PROPOSED ARRANGEMENT OF PARALLEL CHOPPER COMPONENTS